EXPERIMENTAL AND THEORETICAL LOW-SPEED AERODYNAMIC CHARACTERISTICS OF A WORTMANN AIRFOIL AS MANUFACTURED ON A FIBERGLASS SAILPLANE

Dan M. Somers

Langley Research Center
Hampton, Va. 23665

1. Report No. NASA TN D-8324	2. Government Accession No.	3. Recipient's Catalog No.
4. Title and Subtitle EXPERIMENTAL AND THEORETICAL LOW-SPEED AERODYNAMIC CHARACTERISTICS OF A WORTMANN AIRFOIL AS MANUFACTURED ON A FIBERGLASS SAILPLANE		5. Report Date February 1977
		6. Performing Organization Code
7. Author(s) Dan M. Somers		8. Performing Organization Report No. L-10869
9. Performing Organization Name and Address NASA Langley Research Center Hampton, VA 23665		10. Work Unit No. 505-06-31-02
		11. Contract or Grant No.
12. Sponsoring Agency Name and Address National Aeronautics and Space Administration Washington, DC 20546		13. Type of Report and Period Covered Technical Note
		14. Sponsoring Agency Code

15. Supplementary Notes

16. Abstract

An investigation has been conducted in the Langley low-turbulence pressure tunnel to determine the low-speed aerodynamic characteristics of the Wortmann FX 66-17AII-182 airfoil as manufactured on a fiberglass sailplane. The results are compared with data for the design coordinates obtained from another low-turbulence wind tunnel and with theoretical calculations generated by a viscous-flow airfoil computer program. The investigation was performed over a Reynolds number range, based on airfoil chord, of approximately 0.5×10^6 to 6.0×10^6 and a Mach number range of about 0.05 to 0.35. Comparison with data from another wind tunnel for the design coordinates showed slightly higher drag for the manufactured section.

17. Key Words (Suggested by Author(s)) Airfoils Sailplanes Laminar flow	18. Distribution Statement Unclassified - Unlimited Subject Category 02

19. Security Classif. (of this report) Unclassified	20. Security Classif. (of this page) Unclassified	21. No. of Pages 48	22. Price* $3.75

EXPERIMENTAL AND THEORETICAL LOW-SPEED AERODYNAMIC CHARACTERISTICS

OF A WORTMANN AIRFOIL AS MANUFACTURED ON A FIBERGLASS SAILPLANE

Dan M. Somers
Langley Research Center

SUMMARY

An investigation was conducted in the Langley low-turbulence pressure tunnel to determine the basic low-speed, two-dimensional aerodynamic characteristics of the Wortmann FX 66-17AII-182 airfoil as manufactured on a fiberglass sailplane. The results are compared with data from another low-turbulence wind tunnel and with theoretical calculations generated by a viscous-flow airfoil computer program. The investigation was performed over a Reynolds number range, based on airfoil chord, of approximately 0.5×10^6 to 6.0×10^6 and a Mach number range of about 0.05 to 0.35.

The results indicate that maximum lift coefficient decreased with increasing Reynolds number up to about 3.0×10^6, beyond which it increased with increasing Reynolds number. Separation occurred from the trailing edge forward. Minimum drag coefficient decreased with increasing Reynolds number. Maximum lift coefficient increased with increasing Mach number whereas minimum drag coefficient remained essentially constant. Comparison with data obtained from another wind tunnel for the design coordinates showed slightly higher drag for the manufactured section. The deficiencies were attributed to differences between the coordinates of the manufactured and the design sections, probably caused by fiberglass construction techniques. Comparisons with calculated results from a viscous-flow method were good for chordwise pressure distributions and lift and pitching-moment coefficients where no separation was present. The theoretical drag coefficients, however, were generally high for positive lift coefficients and low for negative lift coefficients.

INTRODUCTION

Research on advanced technology airfoils has received considerable attention over the past several years at the Langley Research Center. The particular airfoil tested in this experiment was selected because of the availability of data from another low-turbulence wind tunnel and because it is representative of state-of-the-art, single-element, laminar airfoils of fixed geometry (i.e., no flap). A further objective was to determine the effects of practical fiberglass construction techniques on the aerodynamic characteristics of the airfoil. Accordingly, the wind-tunnel model was built to coordinates measured from templates of a fiberglass sailplane wing. The airfoil corresponds to the FX 66-17AII-182 designed by Professor F. X. Wortmann of the University of Stuttgart, West Germany. The experimental section characteristics of the FX 66-17AII-182 airfoil are reported in reference 1.

The investigation was performed in the Langley low-turbulence pressure tunnel (ref. 2) to obtain the basic low-speed, two-dimensional aerodynamic characteristics of the airfoil. The results have been compared with data from reference 1 and with theoretical data generated by a viscous, subsonic airfoil computer program. During the test, the Reynolds number, based on airfoil chord, varied from approximately 0.5×10^6 to 6.0×10^6 over a Mach number range from about 0.05 to 0.35. The geometric angle of attack varied from $-10°$ to $15°$.

SYMBOLS

Values are given in both SI and U.S. Customary Units. Measurements and calculations were made in U.S. Customary Units.

C_p pressure coefficient, $\dfrac{p_l - p_\infty}{q_\infty}$

c airfoil chord, cm (in.)

c_c section chord-force coefficient, $\oint C_p \, d\left(\dfrac{z}{c}\right)$

c_d section profile-drag coefficient, $\displaystyle\int_{wake} c_d{}' \, d\left(\dfrac{h}{c}\right)$

$c_d{}'$ point drag coefficient (ref. 3)

c_l section lift coefficient, $c_n \cos \alpha - c_c \sin \alpha$

c_m section pitching-moment coefficient about quarter-chord point,

$$-\oint C_p\left(\dfrac{x}{c} - 0.25\right) d\left(\dfrac{x}{c}\right) + \oint C_p\left(\dfrac{z}{c}\right) d\left(\dfrac{z}{c}\right)$$

c_n section normal-force coefficient, $-\oint C_p \, d\left(\dfrac{x}{c}\right)$

h vertical distance in wake profile, cm (in.)

M free-stream Mach number

p static pressure, Pa (lb/ft^2)

q dynamic pressure, Pa (lb/ft^2)

R Reynolds number based on free-stream conditions and airfoil chord

x airfoil abscissa, cm (in.)

z airfoil ordinate, cm (in.)

α angle of attack, deg

2

Subscripts:

ι   local point on airfoil

max   maximum

min   minimum

T   transition

∞   free-stream conditions

Abbreviations:

L.S.   lower surface

LTPT   low-turbulence pressure tunnel

U.S.   upper surface

MODEL, APPARATUS, AND PROCEDURE

Model

The coordinates for the wind-tunnel model, which were obtained from templates of a fiberglass sailplane wing, and those for the FX 66-17AII-182 airfoil designed by Wortmann (called design) are presented in table I. The two airfoil section shapes, model and design, compared favorably along the upper surface except near the leading edge, where the model is thinner than the design. The lower surface of the model is considerably thicker than that of the design. (See fig. 1.)

The model consisted of a metal spar surrounded by plastic filler with fiberglass forming the aerodynamic surface and had a chord of 45.77 cm (18.02 in.) and a span of 91.44 cm (36.00 in.). Upper- and lower-surface orifices were located 2.54 cm (1.00 in.) to one side of the midspan at the chord stations indicated in table II. Spanwise orifices were located in the upper surface only to monitor the two-dimensionality of the flow at high angles of attack. The model surface was sanded in the chordwise direction with No. 600 dry silicon carbide paper to insure an aerodynamically smooth finish.

Wind Tunnel

The Langley low-turbulence pressure tunnel (ref. 2) is a closed-throat, single-return tunnel which can be operated at stagnation pressures from 10.13 to 1013 kPa (0.1 to 10 atm) with maximum tunnel-empty test-section Mach numbers of 0.46 and 0.23, respectively. The minimum unit Reynolds number is approximately 0.66×10^6 per meter (0.20×10^6 per foot) at a Mach number of about 0.10, whereas the maximum unit Reynolds number is approximately 49×10^6 per meter

$(15 \times 10^6$ per foot) at a Mach number of 0.23. The test section is 91.44 cm (3.000 ft) wide by 228.6 cm (7.500 ft) high.

Hydraulically actuated circular plates provide positioning and attachment for the two-dimensional model. The plates, 101.6 cm (40.00 in.) in diameter, are flush with the tunnel sidewalls and rotate with the model. The model ends were mounted to rectangular model attachment plates (fig. 2) such that the center of rotation of the circular plates coincided with the quarter-chord point. The gaps between the rectangular plates and the circular plates were closed with flexible sliding metal seals, as shown in figure 2.

Wake Survey Rake

A fixed wake survey rake (fig. 3) was cantilevered from the tunnel sidewall at the model midspan and approximately 1.6 chords downstream from the trailing edge of the model. The wake rake employed 91 total-pressure tubes, 0.152 cm (0.060 in.) in diameter, and 5 static-pressure tubes, 0.318 cm (0.125 in.) in diameter. The total-pressure tubes were flattened to 0.102 cm (0.040 in.) for 0.61 cm (0.24 in.) from the tip of the tube. Each static-pressure tube had four flush orifices located 90° apart, 8 tube diameters from the tip of the tube in the measurement plane of the total-pressure tubes.

Instrumentation

Measurements of the static pressures on the model surfaces and the wake-rake pressures were made by an automatic pressure-scanning system utilizing variable-capacitance precision transducers. Basic tunnel pressures were measured with precision quartz manometers. Geometric angle of attack was measured by a calibrated digital shaft encoder driven by a pinion gear and rack attached to the circular plates. Data were obtained by a high-speed data-acquisition system and were recorded on magnetic tape.

Tests and Methods

The airfoil was tested at Mach numbers from about 0.05 to 0.35 over an angle-of-attack range from -10° to 15°. Reynolds number based on the airfoil chord was varied from approximately 0.5×10^6 to 6.0×10^6.

For several test runs, the model upper surface was coated with oil to determine the location as well as the nature of the boundary-layer transition from laminar to turbulent. Transition was also located by connecting a stethoscope to individual orifices on the model. This allowed an observer to start at the leading edge and progress from orifice to orifice toward the trailing edge. The beginning of the turbulent boundary layer was detected as an increase in noise level over that for the laminar boundary layer.

The static-pressure measurements at the airfoil surface were reduced to standard pressure coefficients and machine integrated to obtain section normal-force and chord-force coefficients and section pitching-moment coefficients

about the quarter-chord. Section profile-drag coefficients were computed from the wake-rake total and the wake-rake static pressures by the method of reference 3.

The effect on section data of the standard low-speed wind-tunnel boundary corrections (ref. 4) is shown in figure 4. The corrections, approximately 1 percent of the measured coefficients, have been applied to the data.

PRESENTATION OF RESULTS

All the results shown are model smooth. Section characteristics for some Reynolds numbers have been omitted to make the figures more readable. The principal results of this investigation are presented in the following figures:

DISCUSSION OF RESULTS

Experimental Results

Pressure distributions.- The effect of angle of attack on chordwise pressure distribution at a Reynolds number of approximately 1.5×10^6 and a Mach number of 0.10 is shown in figure 5. At an angle of attack of $0°$ ($c_l \approx 0.4$), favorable pressure gradients existed on both surfaces to about $x/c = 0.35$. (See fig. 5(c).) The lower limit of the laminar low-drag range occurred at $\alpha \approx -2°$ ($c_l \approx 0.2$), where a small pressure peak formed on the lower surface near the leading edge. (See fig. 5(b).) The development of this peak signaled the rapid forward movement of the transition point and the loss of all laminar flow on that surface. The upper limit of the low-drag range corresponded roughly to $\alpha \approx 7°$ ($c_l \approx 1.2$), where a pressure peak appeared on the upper surface near the leading edge. (See fig. 5(g).) This pressure peak increased with increasing angle of attack. Consequently, the transition point moved rapidly forward and resulted in a thickening of the boundary layer on the aft portion of the airfoil. This ultimately led to turbulent trailing-edge separation (fig. 5(j)) at $\alpha \approx 10°$. The maximum lift coefficient, approximately 1.4, occurred with completely attached flow (fig. 5(i)) at an angle of attack of about $9°$.

Transition location.- The mechanism of the boundary-layer transition from laminar to turbulent was a laminar separation bubble, identified as "transition" in figure 6. The bubble was caused by a slight adverse pressure gradient (fig. 7) immediately downstream of the minimum pressure on the airfoil upper surface. This slight adverse gradient was a design feature of the airfoil, as discussed in reference 5.

The variation of section lift coefficient with transition location, as determined by stethoscope measurements, is shown in figure 8. Because the stethoscope is connected to individual orifices on the model, the transition location can only be determined as lying somewhere between two adjacent orifices. In figure 7, the symbols represent orifice locations and the faired curves reflect the nature of the discrete measurements taken with the stethoscope, in that each curve has been fitted between the preceding orifice and the one at which turbulent flow was detected. The transition point progressed slowly forward with increasing lift coefficient on the upper surface, whereas the opposite held for the lower surface.

Reynolds number effects.- At a lift coefficient of 0.7, the transition location moved forward approximately 0.05 x/c on the upper surface and 0.06 x/c on the lower surface as the Reynolds number increased from about 0.5×10^6 to about 1.5×10^6. (See fig. 9.) The rates of change of transition location with lift coefficient were comparable for the two Reynolds numbers.

The angle of attack for zero lift coefficient, approximately $-3.7°$, was unaffected by Reynolds number as shown in figure 10. The lift-curve slope increased slightly with increasing Reynolds number at a constant Mach number of 0.10, an increase from about 0.11 per degree at a Reynolds number of approximately 0.5×10^6 to about 0.12 at approximately 3.0×10^6. The pitching moment was relatively insensitive to Reynolds number variation.

At a constant Mach number of 0.10, the maximum lift coefficient decreased as Reynolds number was increased, from about 1.45 at a Reynolds number of approximately 0.5×10^6 to about 1.32 at a Reynolds number of approximately 3.0×10^6 (fig. 11). At Reynolds numbers above about 3.0×10^6, the maximum lift coefficient increased with increasing Reynolds number to about 1.44 at a Reynolds number of approximately 6.0×10^6. The initial decrease and later increase of maximum lift coefficient with increasing Reynolds number was attributed to two different Reynolds number effects on the upper-surface boundary layer. First, as Reynolds number increased from approximately 0.5×10^6 to 3.0×10^6, the transition point moved forward (fig. 9) which resulted in a longer and thus thicker turbulent boundary layer, and in turn led to earlier separation. Separation occurred from the trailing edge forward (i.e., no leading-edge stall). Second, increasing maximum lift coefficient with increasing Reynolds number occurred when the forward movement of the transition location slowed sufficiently to allow the thinning effect on the turbulent boundary layer to become dominant.

At a constant Mach number of 0.10, the minimum drag coefficient decreased from 0.0105 at a Reynolds number of approximately 0.5×10^6 to 0.0063 at a Reynolds number of approximately 6.0×10^6 (fig. 12), due to the thinning effect on the boundary layer.

Mach number effects.- The angle of attack for zero lift coefficient, approximately -3.7°, was unaffected by Mach number. (See fig. 13.) The lift-curve slope increased moderately with increasing Mach number at a constant Reynolds number of about 1.5×10^6, an increase from about 0.10 per degree at a Mach number of 0.05 to about 0.11 per degree at a Mach number of 0.25. The pitching moment decreased from approximately -0.087 at a Mach number of 0.05 to about -0.095 at a Mach number of 0.25, both at a lift coefficient of 0.7. This decrease in pitching moment occurred over the entire lift-coefficient range.

The maximum lift coefficient, at a constant Reynolds number of about 1.5×10^6, increased from 1.36 at a Mach number of 0.05 to 1.52 at a Mach number of about 0.35. (See fig. 14.) The rate of increase was approximately 0.05 in lift coefficient per 0.10 in Mach number.

At a constant Reynolds number of about 1.5×10^6, the minimum drag coefficient remained essentially constant at about 0.0084 over the Mach number range of the investigation (fig. 15). The small deviations from this value were attributed to the variation of wind-tunnel turbulence level with Mach number.

Comparison with other data.- The variation of section lift coefficient with transition location at a Reynolds number of approximately 1.5×10^6 compared favorably with the data for the FX 66-17AII-182 (design) from reference 1. (See fig. 16.) It should be noted that the methods used to determine the transition locations reported in reference 1 are more exact than the method used in the present investigation. The rates of variation agreed well, whereas the actual transition locations were forward of those from reference 1. The transition locations at a lift coefficient of 0.7 were about 0.04 x/c forward on the upper surface and 0.02 x/c forward on the lower surface.

The angle of attack for zero lift coefficient from reference 1, approximately -4.7°, was about 1.0° lower than the LTPT data. (See fig. 17(a).) This

difference was attributed to the thicker lower surface of the FX 66-17AII-182 (model) which resulted in an airfoil with less camber. The difference was verified by comparing the two sections theoretically. (See fig. 17(b).) The lift-curve slopes agreed well. The drag coefficients were slightly higher for the manufactured section. The lower drag of the design section was attributed to its being thinner than the FX 66-17AII-182 (model). Above a lift coefficient of approximately 1.0, the FX 66-17AII-182 (design) displayed significantly lower drag coefficients, probably due to the smaller upper-surface leading-edge radius of the FX 66-17AII-182 (model). (See fig. 1.) The model with this smaller radius developed a leading-edge pressure peak earlier, which resulted in forward movement of the transition location at a lower lift coefficient; this also accounts for the lower maximum lift coefficient. The pitching-moment coefficients agreed well for the two sections.

Comparison of Experimental and Theoretical Data

A viscous-flow airfoil method (ref. 6) was used to calculate two chordwise pressure distributions corresponding to data taken in the current wind-tunnel investigation. The theory agreed quite well with experiment over the entire chord (fig. 18), with the major discrepancies occurring at locations corresponding to laminar separation bubbles.

The theoretical variation of section lift coefficient with transition location at a Reynolds number of approximately 1.5×10^6 compared rather poorly with data taken in the current investigation. (See fig. 19.) The rates of variation agreed remarkably well, although the actual transition locations were approximately 0.10 x/c forward of those observed in the wind tunnel. The transition locations at a lift coefficient of 0.7 were about 0.07 x/c forward on the upper surface and about 0.09 x/c forward on the lower surface. These differences were attributed to the fact that the theoretical method does not model the laminar separation bubble. Instead, it merely tests the laminar boundary layer for a transition criterion, and if transition is predicted, a turbulent boundary-layer calculation is initiated. Thus, the method predicts transition as occurring at a specific point instead of over a definite length as occurs in nature.

The agreement between theoretical and experimental lift and pitching-moment coefficients was excellent (fig. 20) where no separation was present. The theoretical drag coefficients were generally high for positive lift coefficients and low for negative lift coefficients. The minimum drag coefficients, however, were comparable.

SUMMARY OF RESULTS

An investigation was performed in the Langley low-turbulence pressure tunnel to determine the basic low-speed, two-dimensional aerodynamic characteristics of the Wortmann FX 66-17AII-182 airfoil as manufactured on a fiberglass sailplane. The resulting data have been compared with data from another low-turbulence wind tunnel and with theoretical calculations generated by a viscous-flow airfoil computer program. The investigation was conducted with Reynolds number, based on airfoil chord, varying from approximately 0.5×10^6 to

6.0×10^6, and Mach number varying from about 0.05 to 0.35. The following results were obtained:

1. The maximum lift coefficient, at a constant Mach number of 0.10, decreased from about 1.45 at a Reynolds number of approximately 0.5×10^6 to about 1.32 at approximately 3.0×10^6. At a Reynolds number above about 3.0×10^6, the maximum lift coefficient increased with increasing Reynolds number to about 1.44 at a Reynolds number of approximately 6.0×10^6.

2. Separation occurred from the trailing edge forward (i.e., no leading-edge stall).

3. The minimum drag coefficient decreased, at a constant Mach number of 0.10, from 0.0105 at a Reynolds number of about 0.5×10^6 to 0.0063 at a Reynolds number of about 6.0×10^6.

4. The maximum lift coefficient, at a constant Reynolds number of about 1.5×10^6, increased from 1.36 at a Mach number of 0.05 to 1.52 at a Mach number of about 0.35.

5. The minimum drag coefficient, at a constant Reynolds number of about 1.5×10^6, remained essentially constant at about 0.0084 between the Mach numbers of 0.05 and 0.35.

6. Comparison with data from another wind tunnel for the design coordinates indicated slightly higher drag for the manufactured section.

7. Comparisons with calculated results from a viscous-flow method were good for chordwise pressure distributions and lift and pitching-moment coefficients, where no separation was present. The theoretical drag coefficients, however, were generally high for positive lift coefficients and low for negative lift coefficients. The theoretical transition locations were approximately 0.10 chord forward of those measured in the wind tunnel.

Langley Research Center
National Aeronautics and Space Administration
Hampton, VA 23665
December 22, 1976

9

REFERENCES

1. Althaus, D.: MeBergebnisse aus dem Laminarwindkanal des Instituts für Aero-
   dynamik und Gasdynamik der Universität Stuttgart. Stuttgarter Profilkata-
   log I, Institut für Aerodynamik und Gasdynamik der Universität Stuttgart,
   1972.

2. Von Doenhoff, Albert E.; and Abbott, Frank T., Jr.: The Langley Two-
   Dimensional Low-Turbulence Pressure Tunnel. NACA TN 1283, 1947.

3. Pankhurst, R. C.; and Holder, D. W.: Wind-Tunnel Technique. Sir Issac Pit-
   man & Sons, Ltd. (London), 1952.

4. Allen, H. Julian; and Vincenti, Walter G.: Wall Interference in a Two-
   Dimensional-Flow Wind Tunnel, With Consideration of the Effect of Compressi-
   bility. NACA Rep. 782, 1944. (Supersedes NACA WR A-63.)

5. Wortmann, F. X.: Experimental Investigations on New Laminar Profiles for
   Gliders and Helicopters. TIL/T.4906, British Minist. Aviat., Mar. 1960.

6. Smetana, Frederick O.; Summey, Delbert C.; Smith, Neill S.; and Carden,
   Ronald K.: Light Aircraft Lift, Drag, and Moment Prediction - A Review
   and Analysis. NASA CR-2523, 1975.

TABLE I.- AIRFOIL COORDINATES

[c ▫ 45.7726 cm (18.0207 in.)]

(a) FX 66-17AII-182 (model)

Upper surface		Lower surface	
x/c	z/c	x/c	z/c
0.00000	0.00000	0.00000	0.00000
.00083	.00347	.00083	-.00516
.00166	.00563	.00166	-.00691
.00277	.00786	.00277	-.00856
.00388	.00966	.00388	-.00992
.00499	.01134	.00527	-.01136
.00585	.01259	.00641	-.01231
.01353	.02120	.01352	-.01676
.01781	.02521	.03588	-.02573
.02475	.03106	.05113	-.03040
.03467	.03841	.07643	-.03651
.05013	.04861	.10169	-.04131
.06090	.05510	.15067	-.04833
.07574	.06328	.20055	-.05321
.10199	.07608	.25032	-.05617
.15106	.09548	.30166	-.05779
.20035	.11042	.35047	-.05782
.25320	.12165	.40069	-.05597
.30311	.12819	.45007	-.05253
.35283	.13066	.49998	-.04772
.40185	.12902	.55056	-.04134
.45244	.12335	.59970	-.03396
.50043	.11506	.64952	-.02630
.55178	.10427	.70012	-.01892
.60095	.09328	.74995	-.01234
.65056	.08197	.79808	-.00732
.70137	.07028	.84898	-.00364
.74442	.06026	.89907	-.00133
.80012	.04737	.94758	-.00060
.84997	.03585	.97026	-.00095
.90009	.02433	.97832	-.00104
.94994	.01257	1.00000	-.00059
.97613	.00629		
.99033	.00285		
.99964	.00021		

TABLE I.- Concluded

(b) FX 66-17AII-182 (design)

Upper surface		Lower surface	
x/c	z/c	x/c	z/c
0.00000	0.00000	0.00000	0.00000
.00107	.00616	.00107	-.00340
.00428	.01211	.00428	-.00741
.00961	.01866	.00961	-.01158
.01704	.02686	.01704	-.01514
.02653	.03492	.02653	-.01911
.03806	.04335	.03806	-.02298
.05156	.05201	.05156	-.02674
.06699	.06076	.06699	-.03035
.08427	.06949	.08427	-.03379
.10332	.07805	.10332	-.03702
.12408	.08635	.12408	-.04004
.14645	.09426	.14645	-.04280
.17033	.10169	.17033	-.04532
.19562	.10850	.19562	-.04752
.22221	.11460	.22221	-.04944
.25000	.11984	.25000	-.05098
.27866	.12409	.27866	-.05218
.30866	.12705	.30866	-.05292
.33928	.12874	.33928	-.05321
.37059	.12897	.37059	-.05288
.40245	.12774	.40245	-.05198
.43474	.12492	.43474	-.05037
.46730	.12065	.46730	-.04796
.50000	.11512	.50000	-.04464
.53270	.10873	.53270	-.04050
.56526	.10185	.56526	-.03573
.59755	.09476	.59755	-.03072
.62941	.08755	.62941	-.02575
.66072	.08032	.66072	-.02112
.69134	.07315	.69134	-.01693
.72114	.06614	.72114	-.01326
.75000	.05934	.75000	-.01010
.77779	.05282	.77779	-.00744
.80438	.04662	.80438	-.00522
.82967	.04078	.82967	-.00342
.85355	.03531	.85355	-.00201
.87592	.03026	.87592	-.00097
.91573	.02139	.91573	.00019
.94844	.01396	.94844	.00063
.97347	.00759	.97347	.00068
.99039	.00258	.99039	.00051
.99893	.00016	.99893	.00016
1.00000	.00000	1.00000	.00000

TABLE II.- MODEL ORIFICE LOCATIONS

Upper surface		Lower surface	
x/c	z/c	x/c	z/c
0.00000	0.00000	0.00000	0.00000
.00585	.01259	.00641	-.01231
.01353	.02120	.03588	-.02573
.01781	.02521	.05113	-.03040
.02475	.03106	.07643	-.03651
.03467	.03841	.10169	-.04131
.05013	.04861	.15067	-.04833
.06090	.05510	.20055	-.05321
.07574	.06328	.25032	-.05617
.10199	.07608	.30166	-.05779
.15106	.09548	.35047	-.05782
.20035	.11042	.40069	-.05597
.25320	.12165	.45007	-.05253
.30311	.12819	.49998	-.04772
.35283	.13066	.55056	-.04134
.40185	.12902	.59970	-.03396
.45244	.12335	.64952	-.02630
.50043	.11506	.70012	-.01892
.55178	.10427	.74995	-.01234
.60095	.09328	.79808	-.00732
.65056	.08197	.84898	-.00364
.70137	.07028	.89907	-.00133
.74442	.06026	.94758	-.00080
.80012	.04737	.97026	-.00095
.84997	.03585	.97832	-.00104
.90009	.02433		
.94994	.01257		
.97613	.00629		
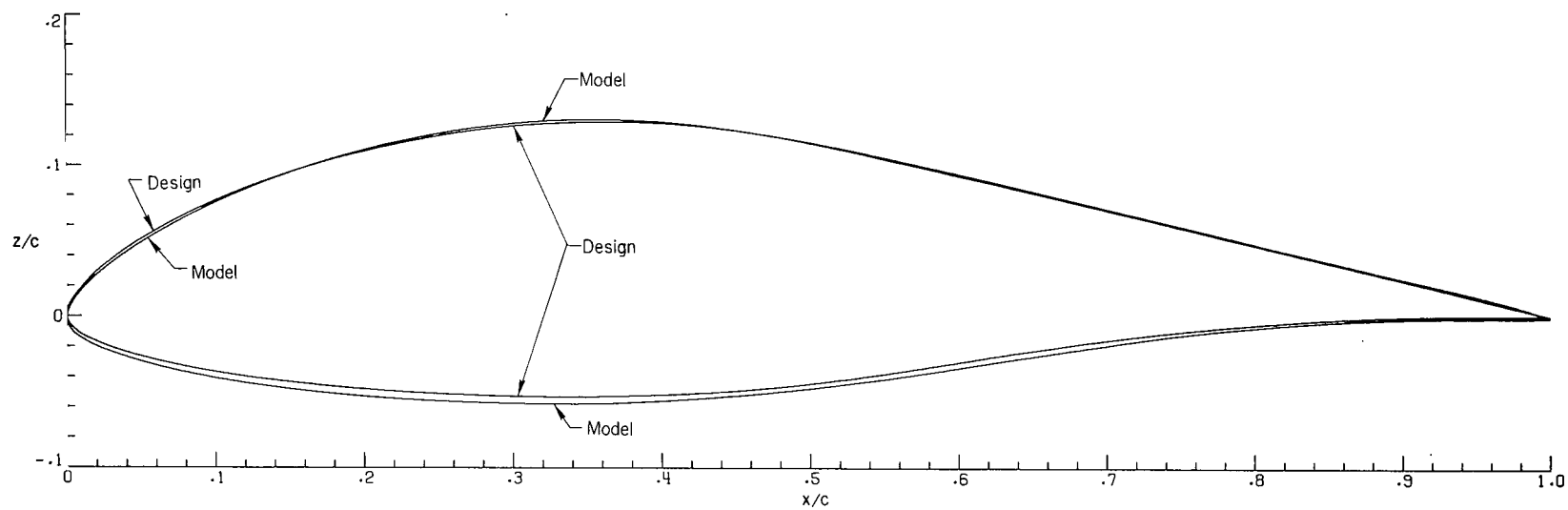
Figure 1.- Comparison of FX 66-17AII-182 (model) and FX 66-17AII-182 (design) coordinates.

Tunnel sidewalls

Diam = 2.22c

Airflow

A

A

2.00c

Circular plate

Metal seals

Seal detail B

B

Top view

Model positioning attachment

Model attachment plate

Zero incidence reference

Tunnel center line

c/4

c

End view, section A—A
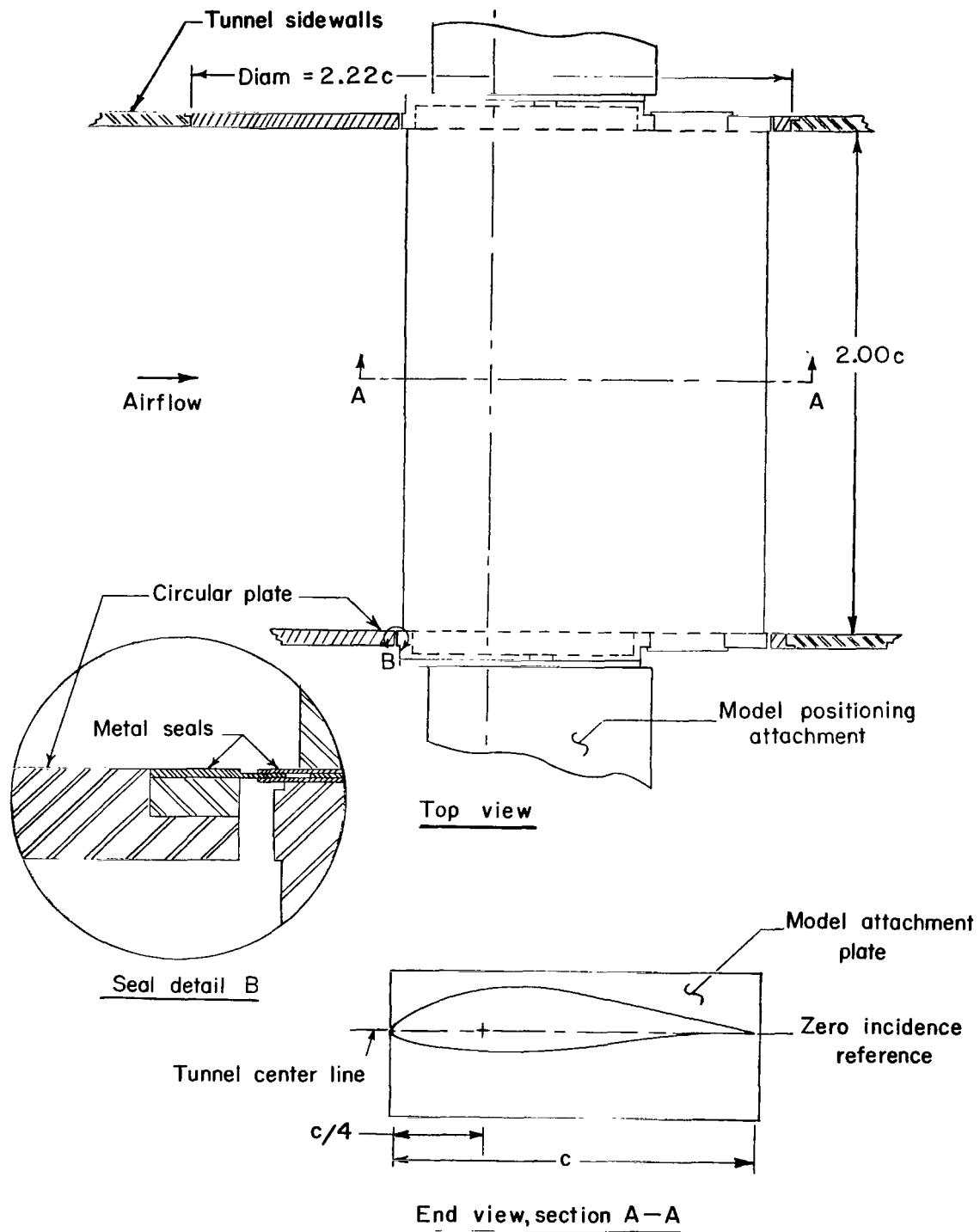
Figure 2.- Airfoil model mounted in wind tunnel. c = 45.77 cm (18.02 in.).
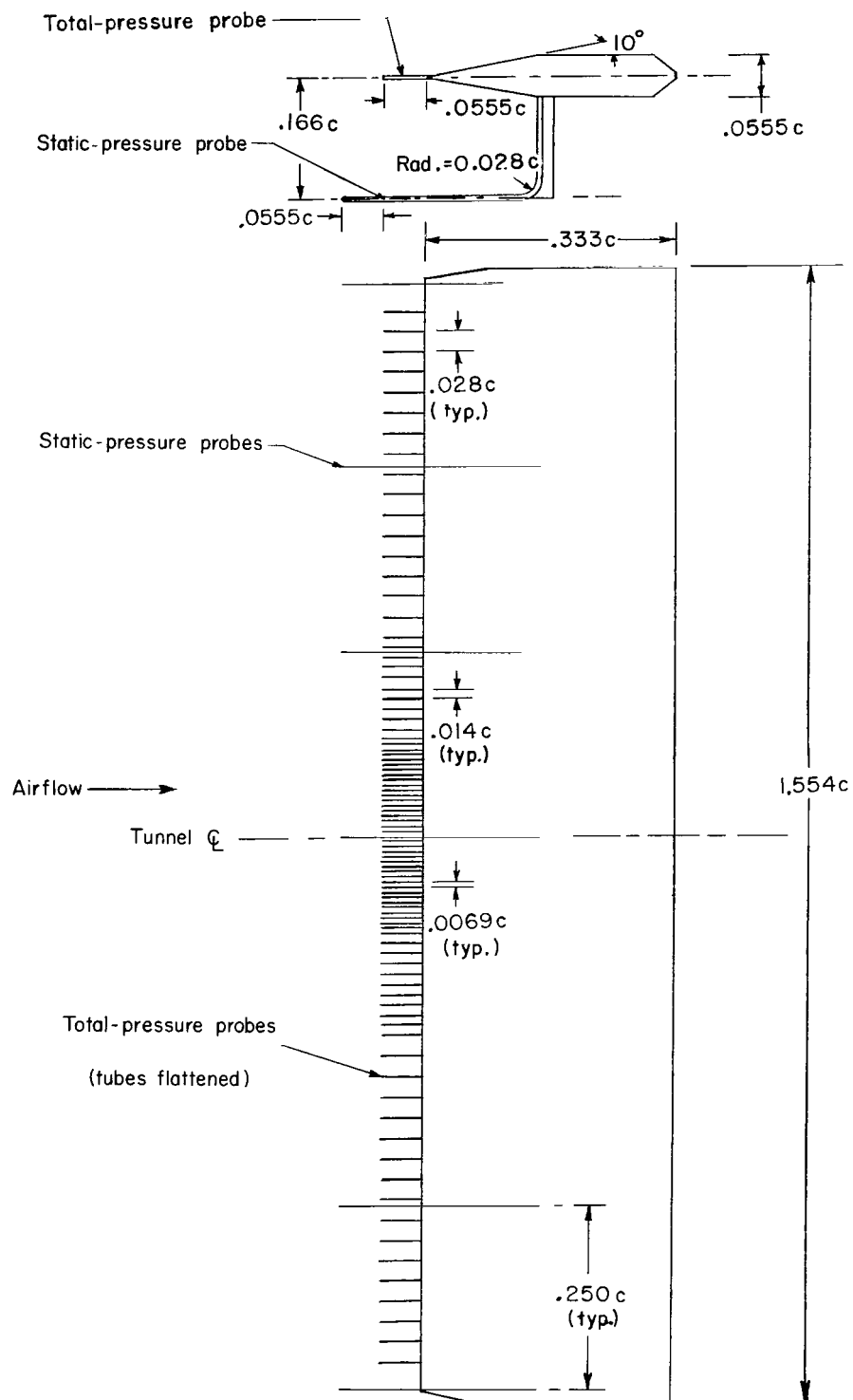
Figure 3.- Wake survey rake. c = 45.77 cm (18.02 in.).
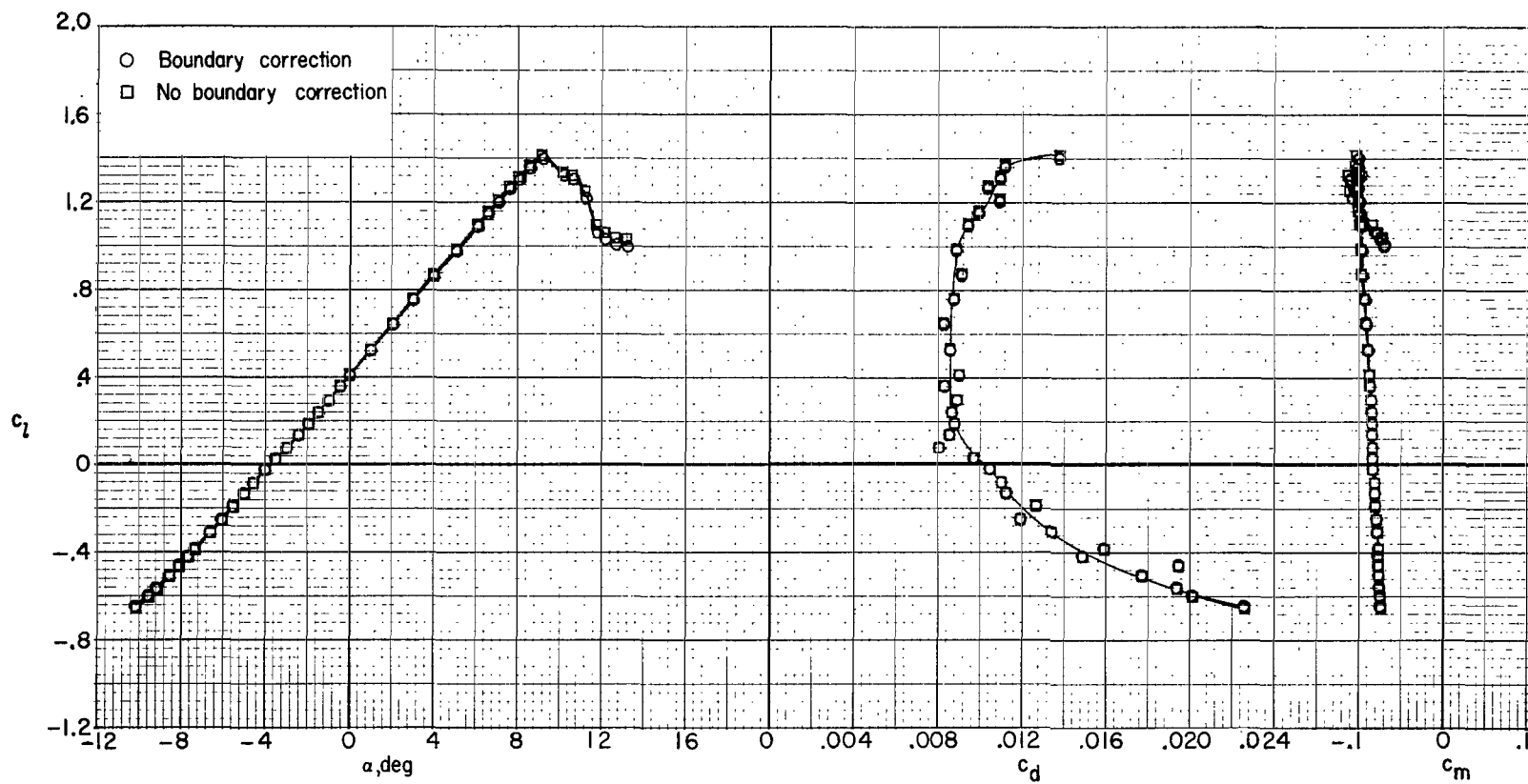
Figure 4.- Effect of standard low-speed wind-tunnel boundary corrections on section data for $R \approx 1.5 \times 10^6$ and $M = 0.10$.
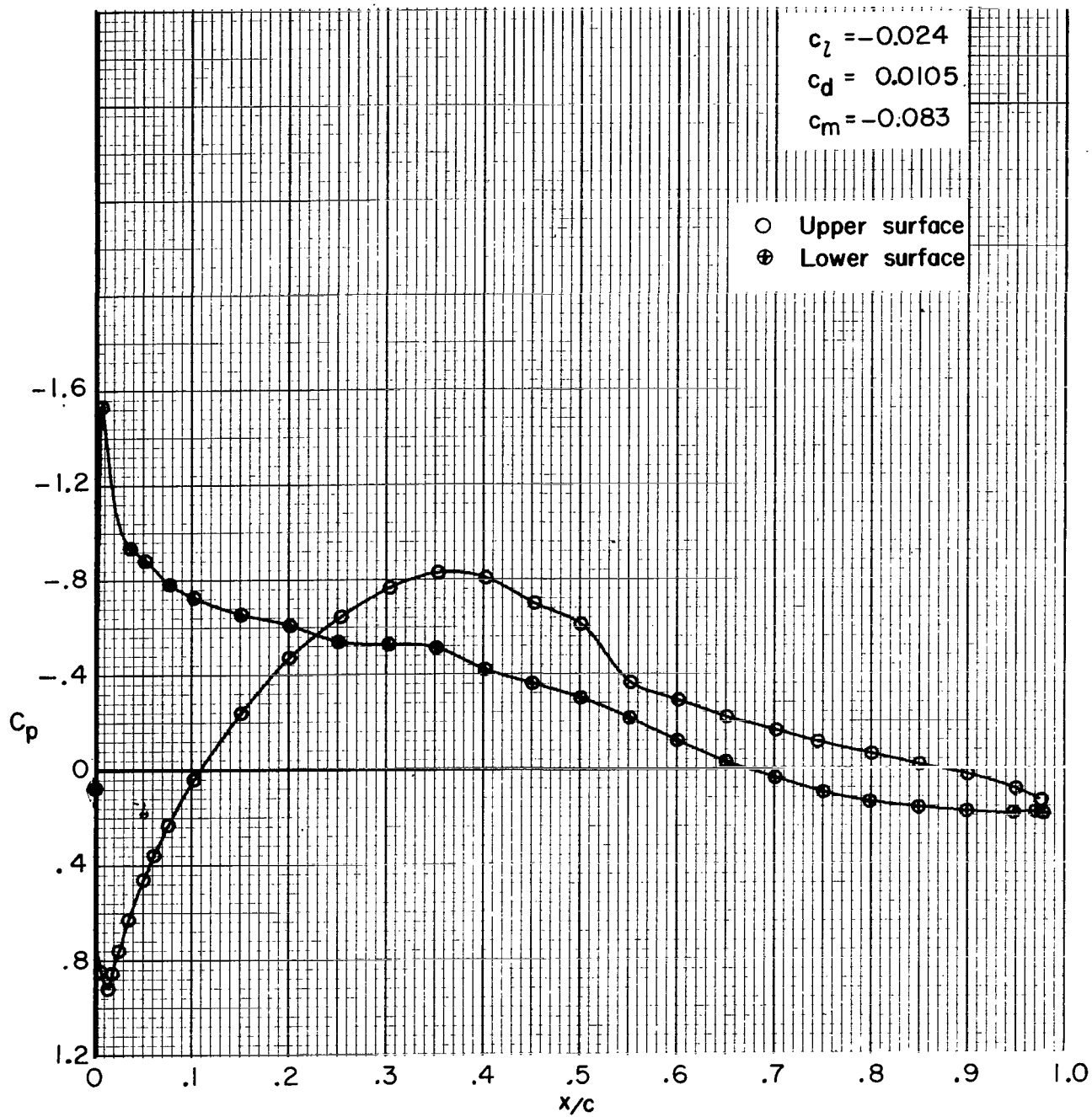
(a) $\alpha = -4.05°$.

Figure 5.- Effect of angle of attack on chordwise pressure distribution for $R \approx 1.5 \times 10^6$ and $M = 0.10$.
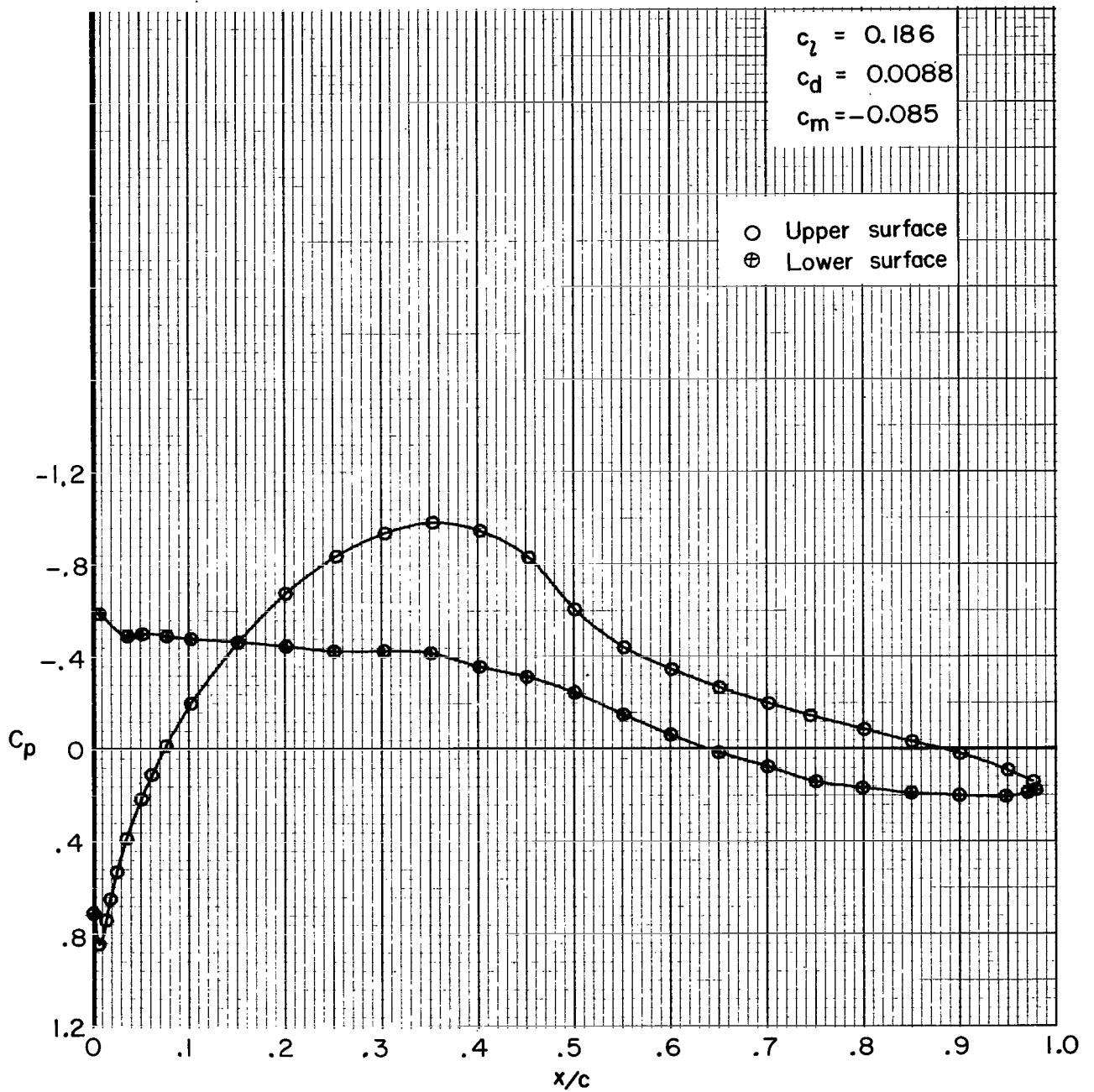
(b) $\alpha = -2.00°$.

Figure 5.- Continued.
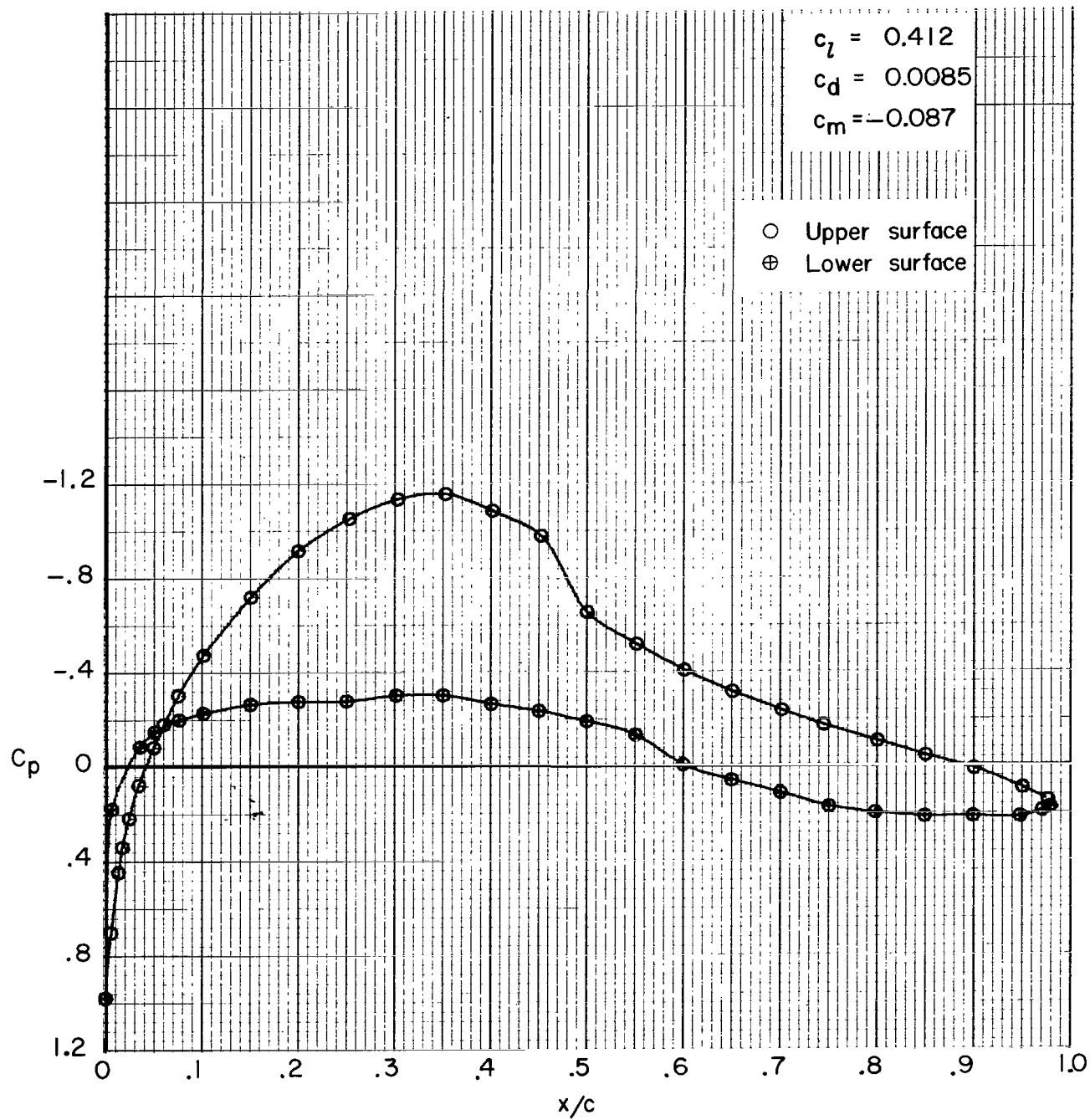
(c) $\alpha = 0.00^{\circ}$.

Figure 5.- Continued.
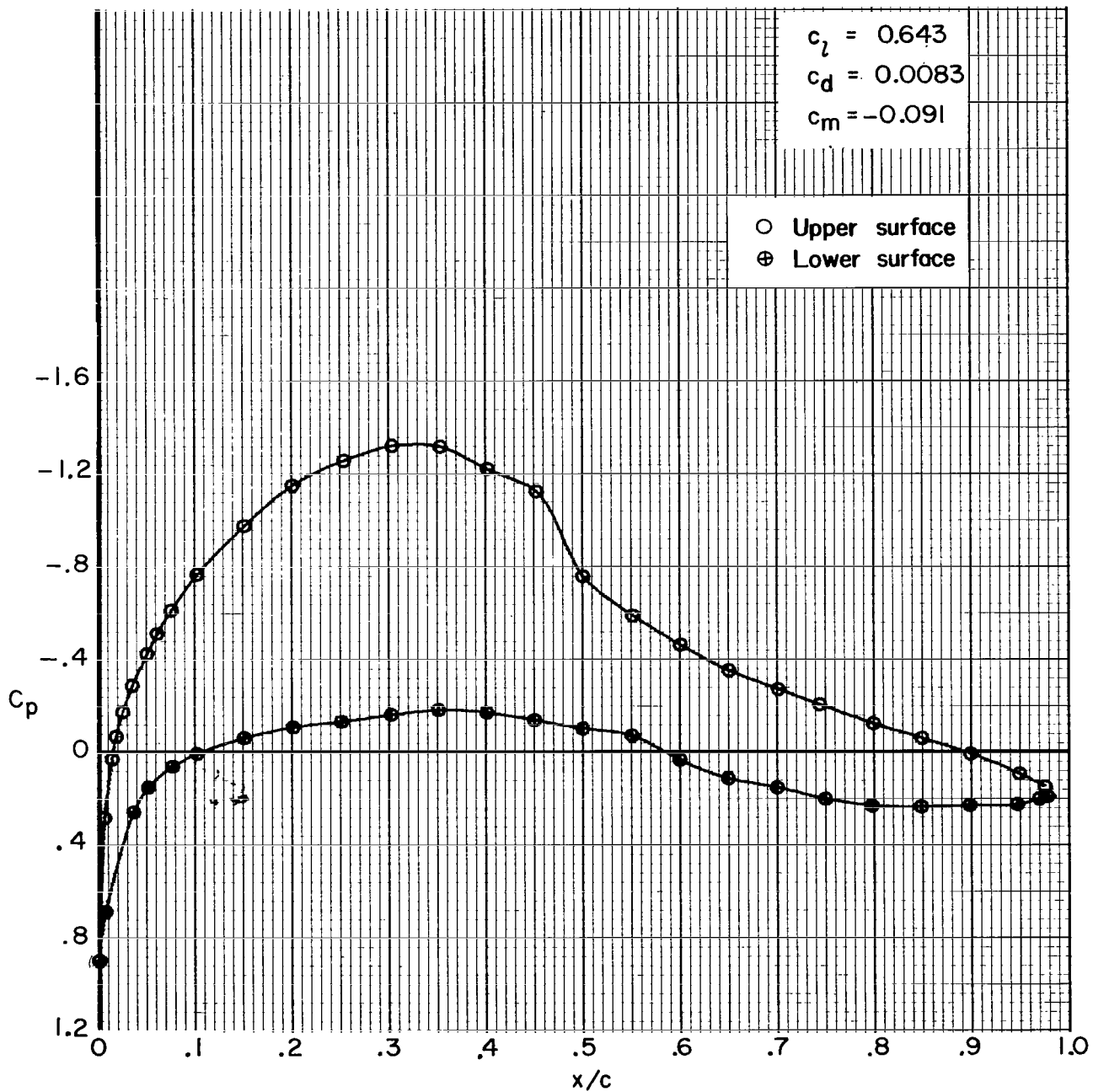
(d) $\alpha = 2.03^{\circ}$.

Figure 5.- Continued.
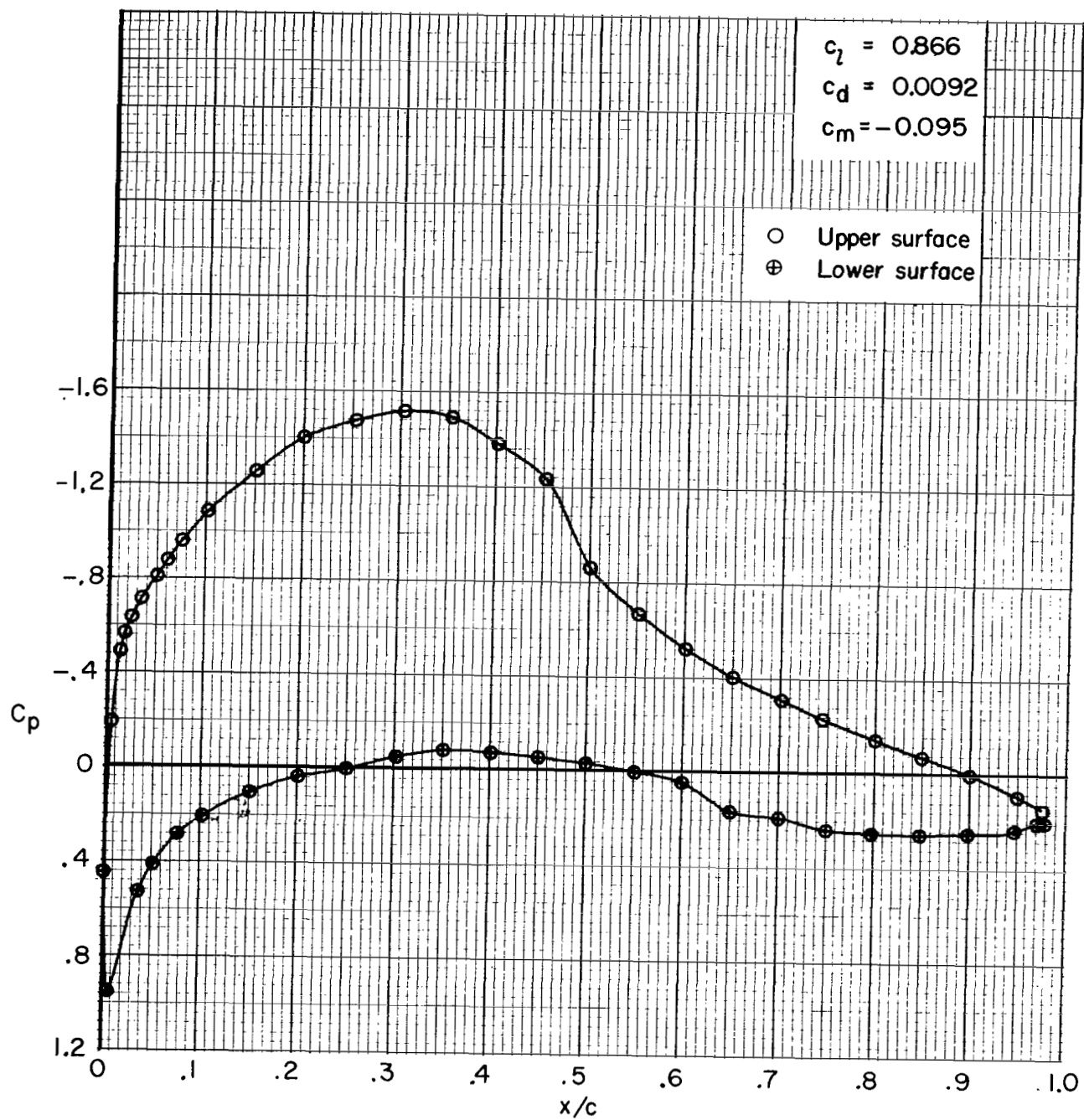
(e) $\alpha = 4.00°$.

Figure 5.- Continued.
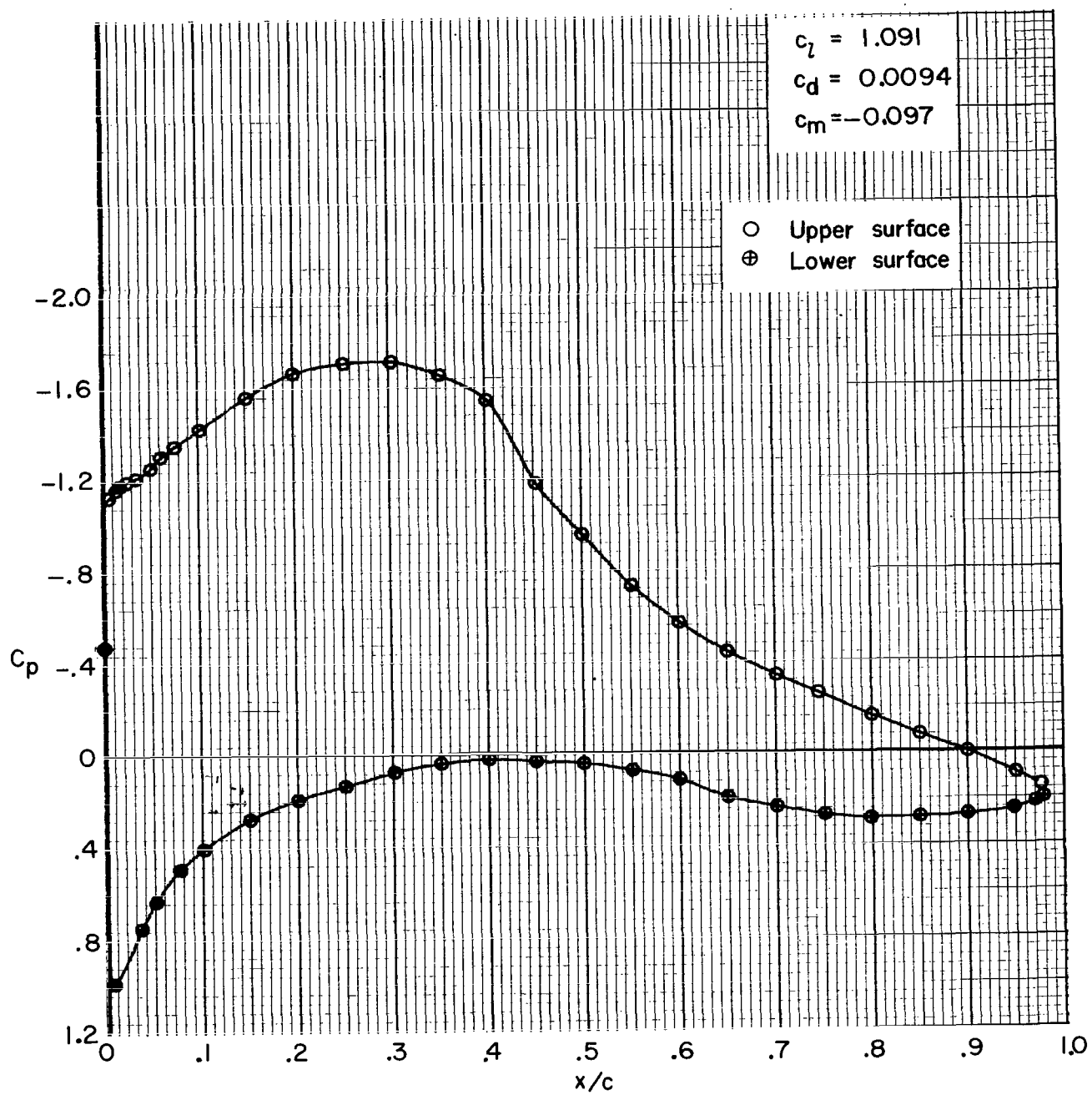
(f) $\alpha = 6.07^{\circ}$.

Figure 5.- Continued.
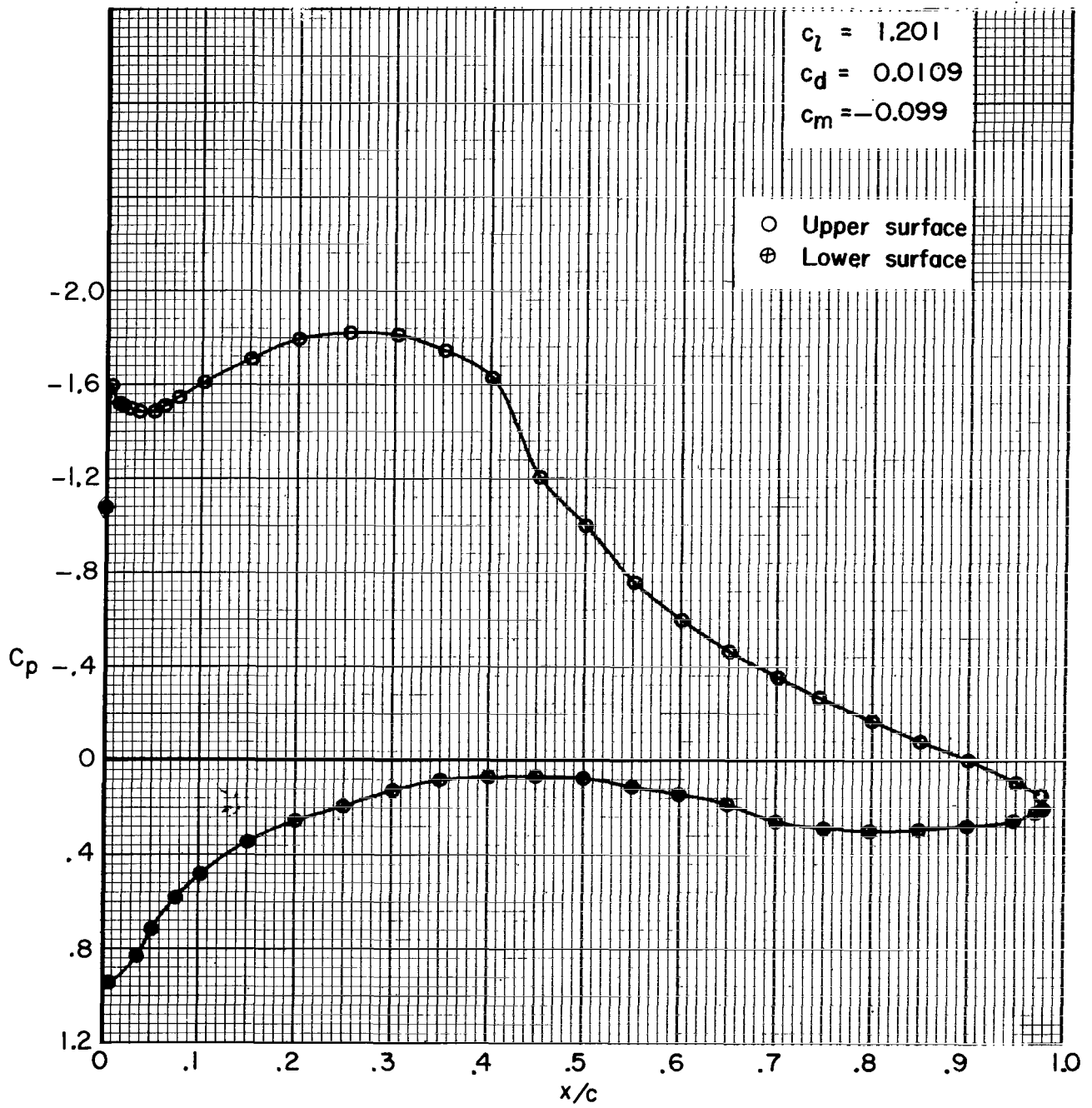
(g) $\alpha = 7.07^{\circ}$.

Figure 5.- Continued.

(h) $\alpha = 8.05^\circ$.

Figure 5.- Continued.

$$c_l = 1.400$$
$$c_d = 0.0138$$
$$c_m = -0.100$$
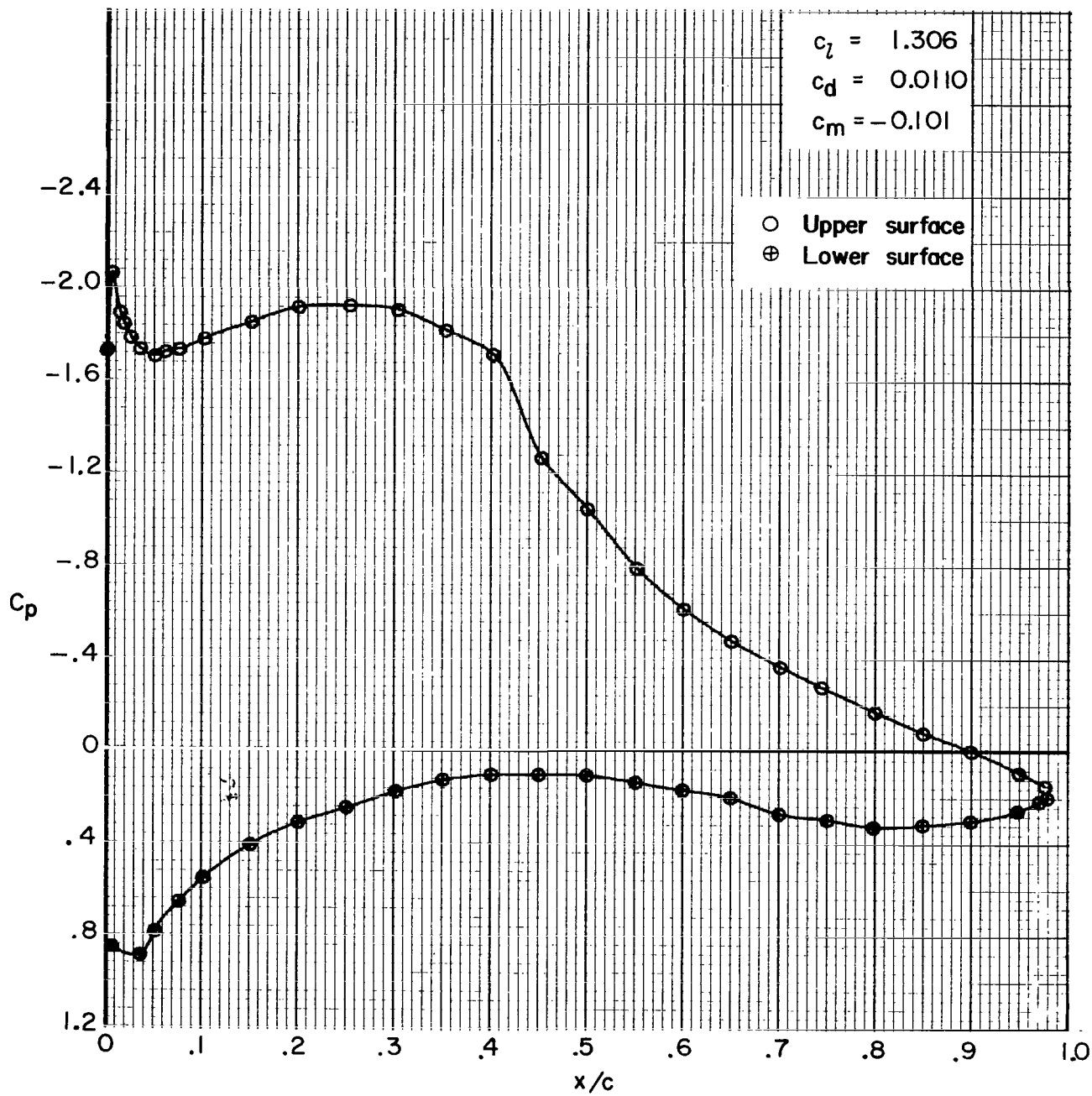
○ Upper surface
⊕ Lower surface
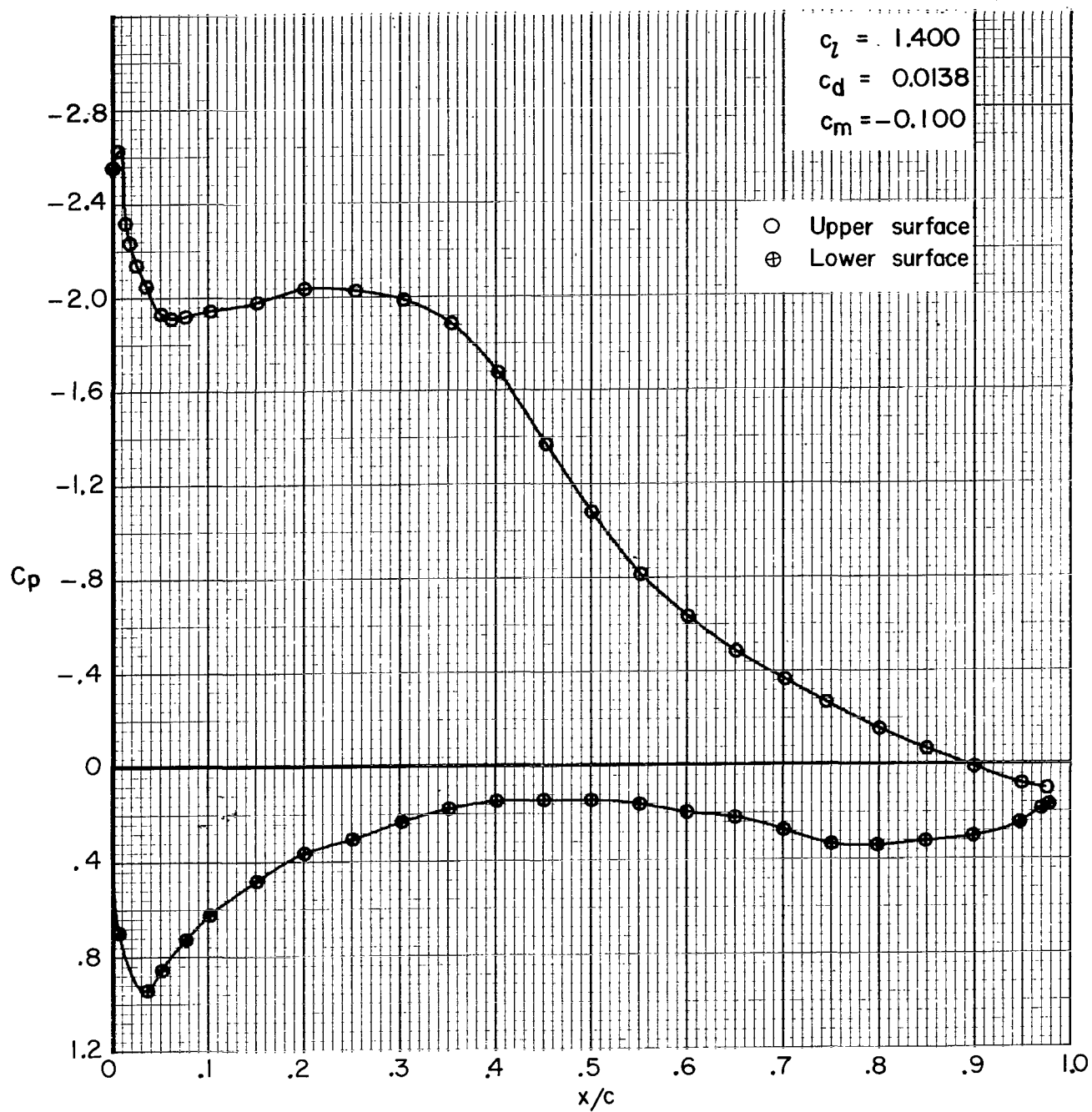
(i) $\alpha = 9.18°$.
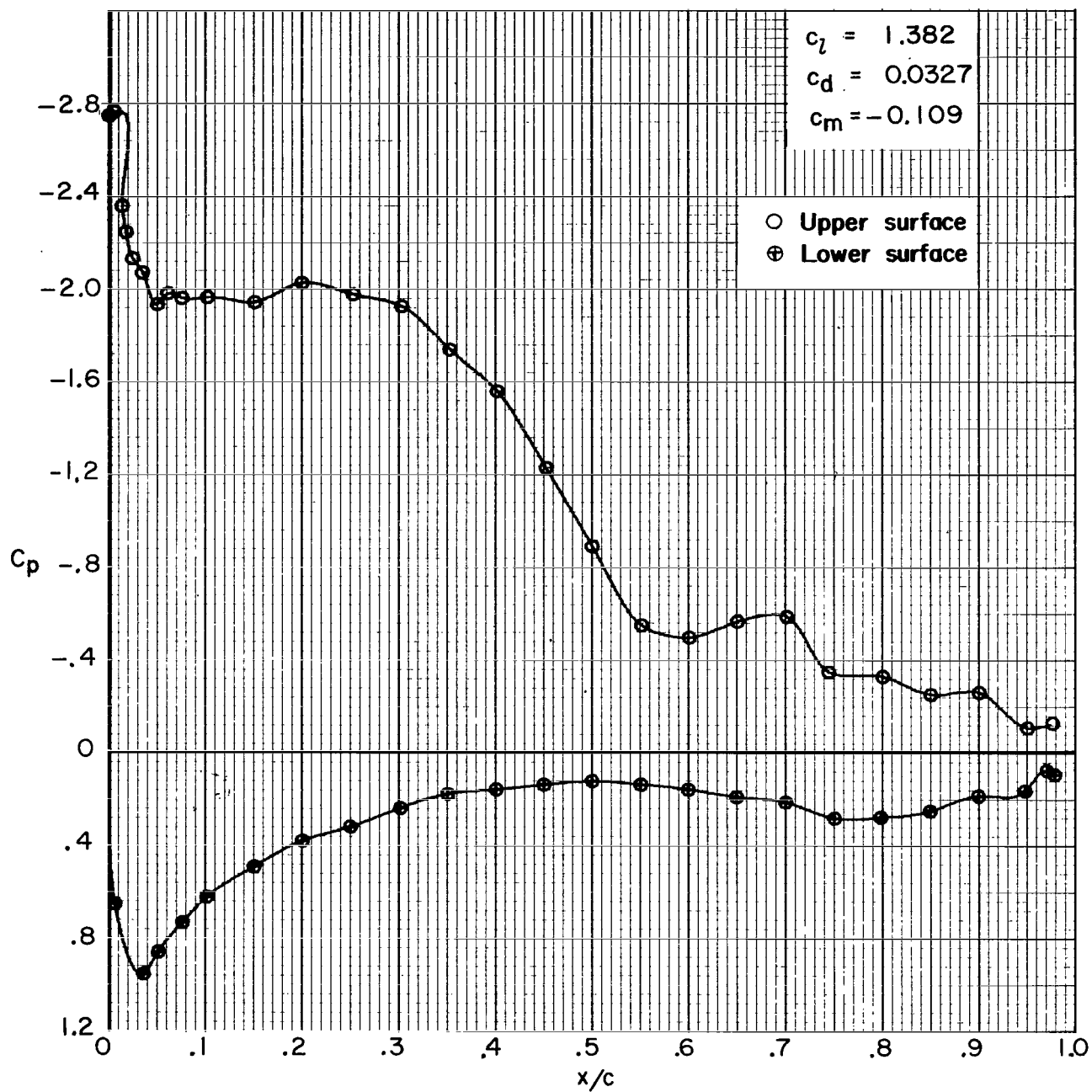
Figure 5.- Continued.

(j) $\alpha = 10.16^{\circ}$.

Figure 5.- Continued.
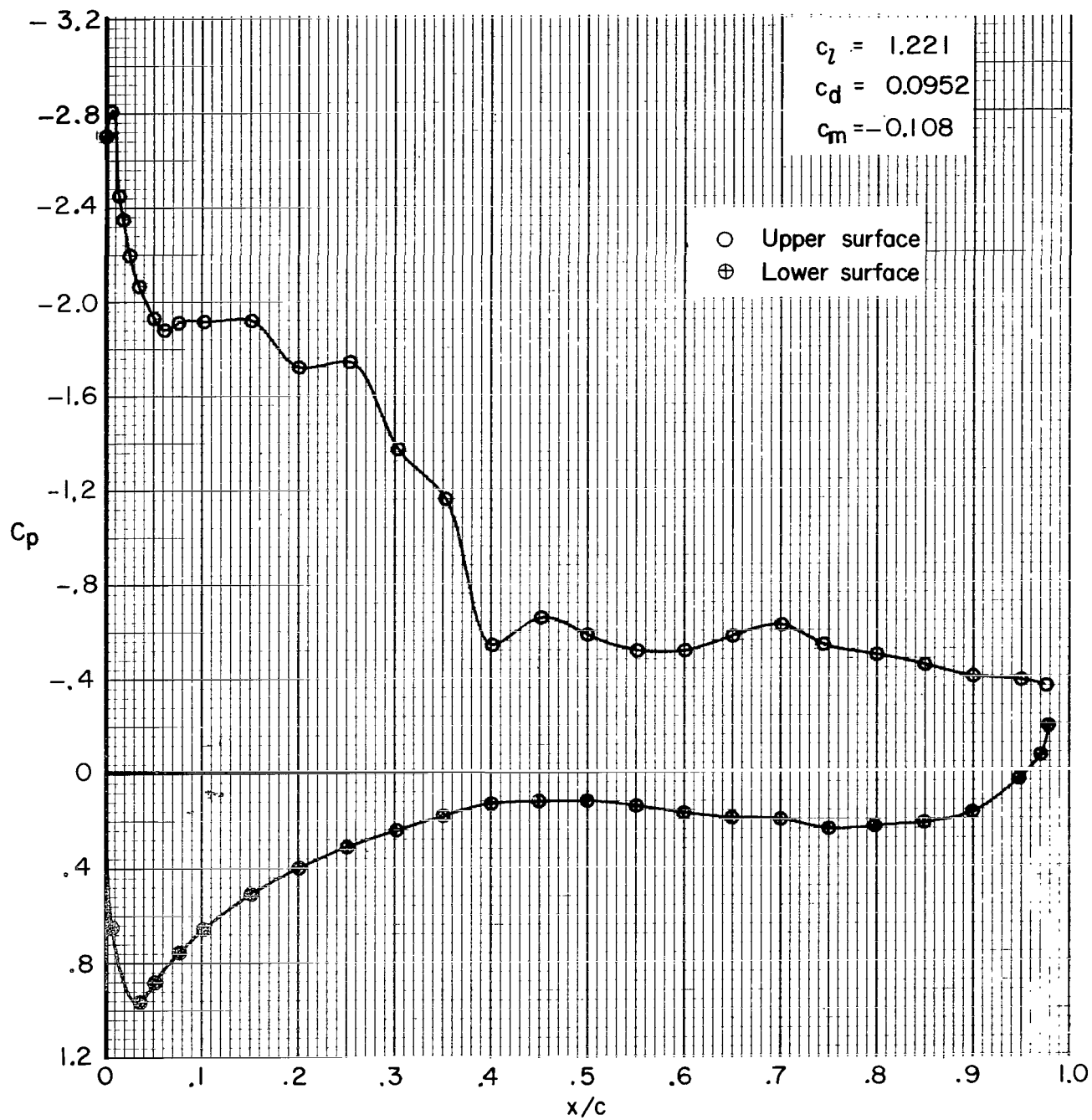
(k) $\alpha = 11.23°$.

Figure 5.- Continued.
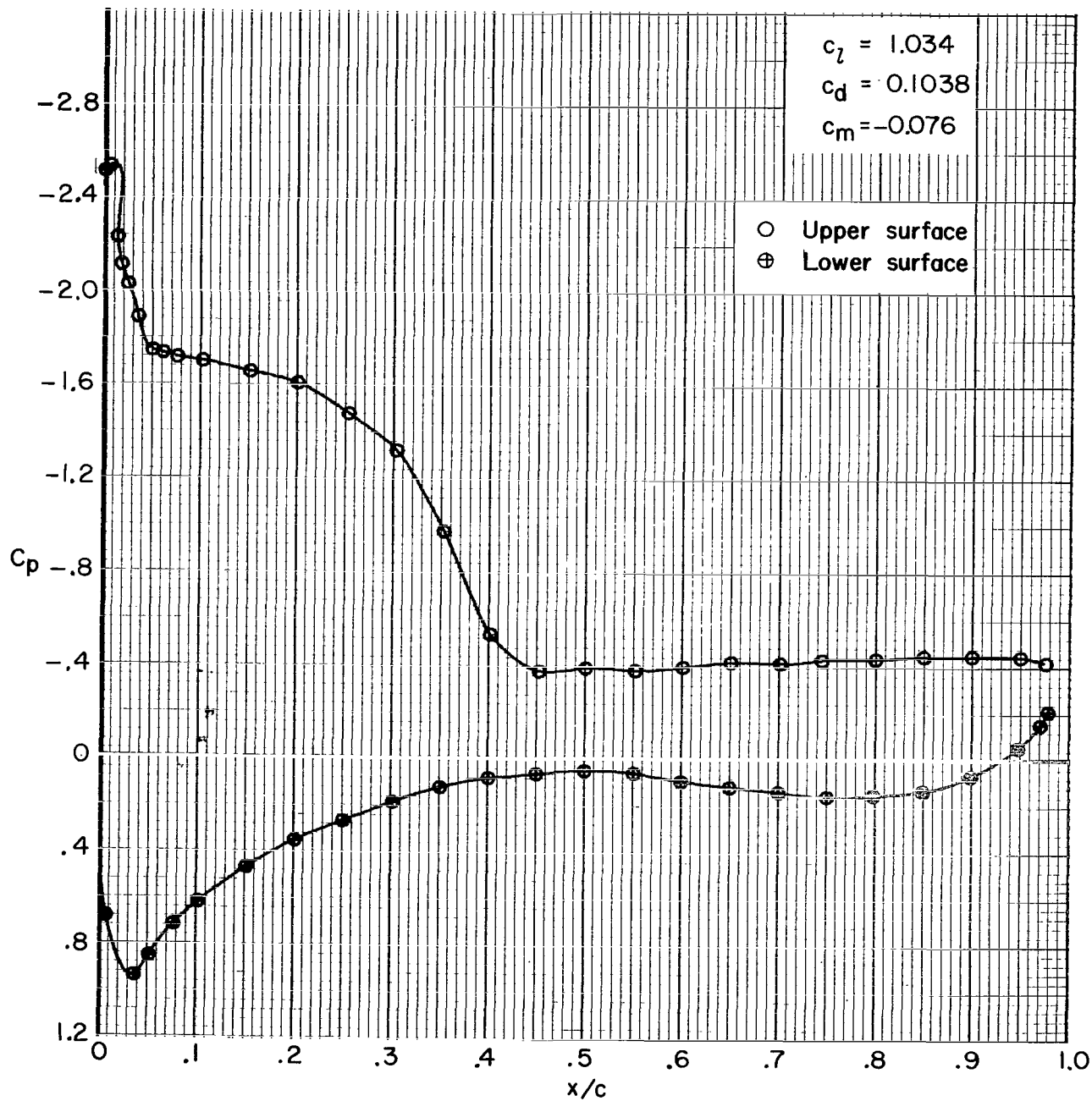
(1) $\alpha = 12.14^{\circ}$.

Figure 5.- Concluded.

Leading edge

Laminar

Transition

Turbulent

Trailing edge
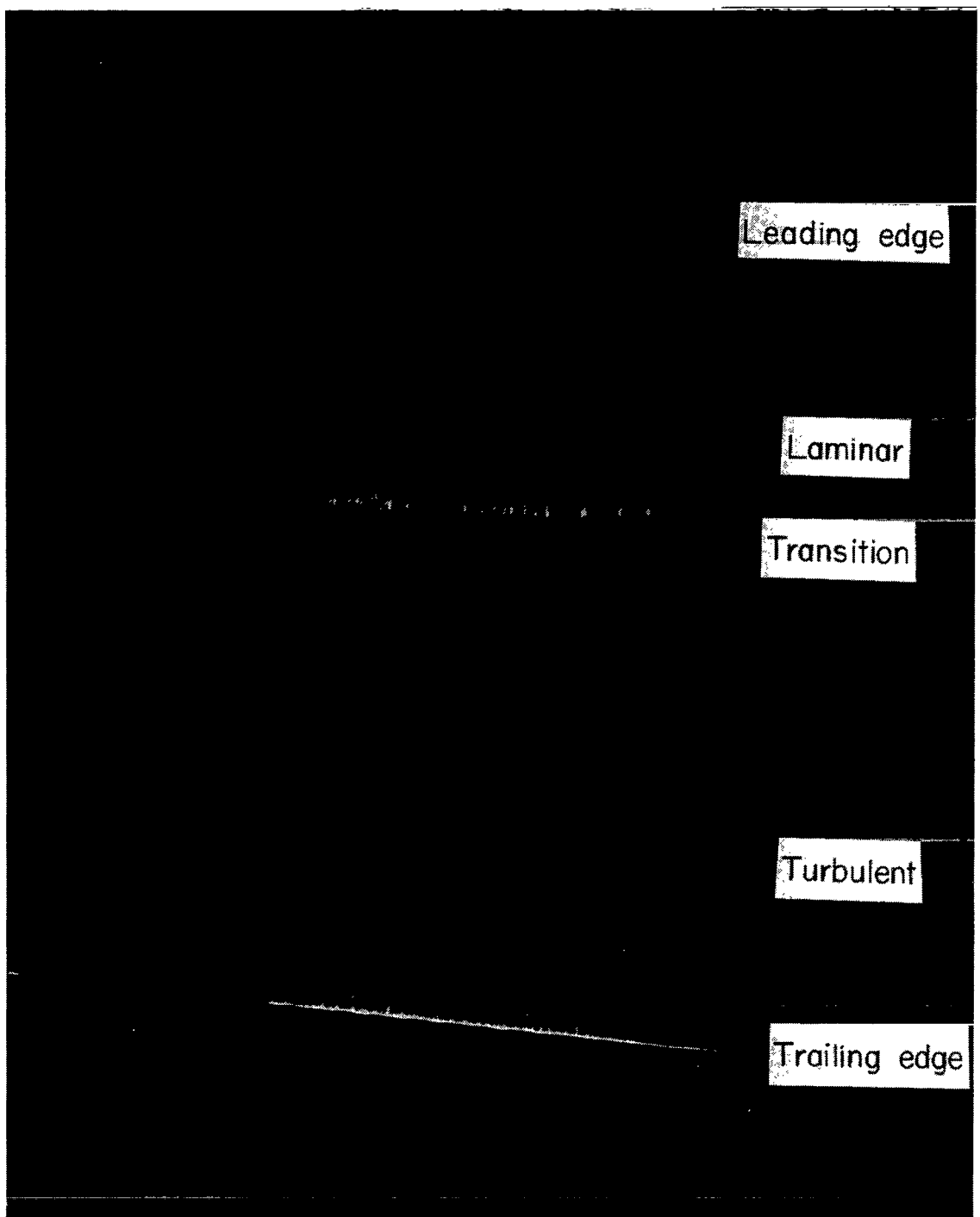
L-77-105

Figure 6.- Oil-flow photograph of upper surface of FX 66-17AII-182 (model) for $R \approx 1.5 \times 10^6$, $M = 0.15$, $\alpha = 0^{\circ}$, and $c_l \approx 0.4$.
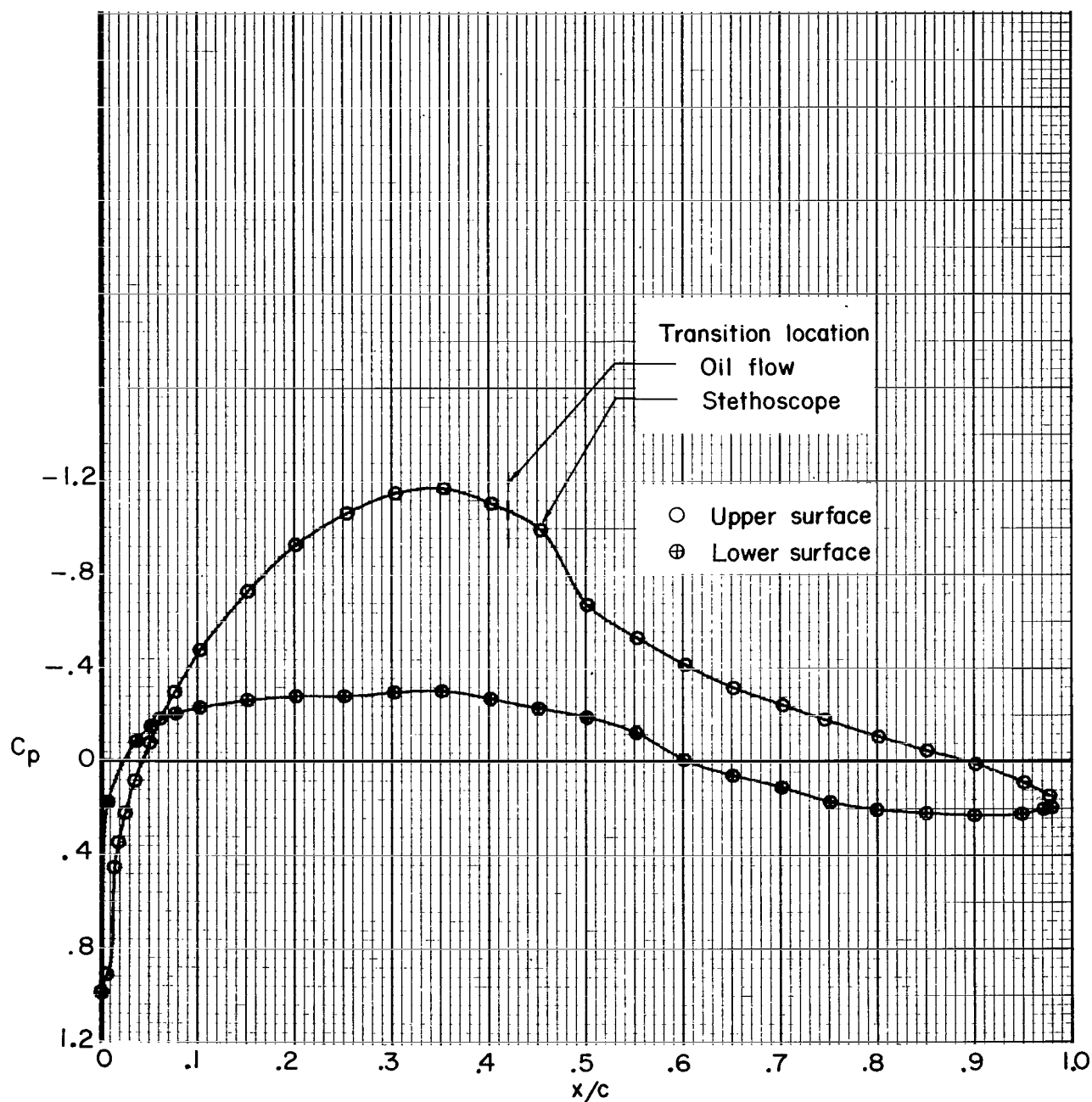
Figure 7.- Effect of chordwise pressure distribution on transition location for $R \approx 1.5 \times 10^6$, $M = 0.15$, $\alpha = 0^\circ$, and $c_l \approx 0.4$.
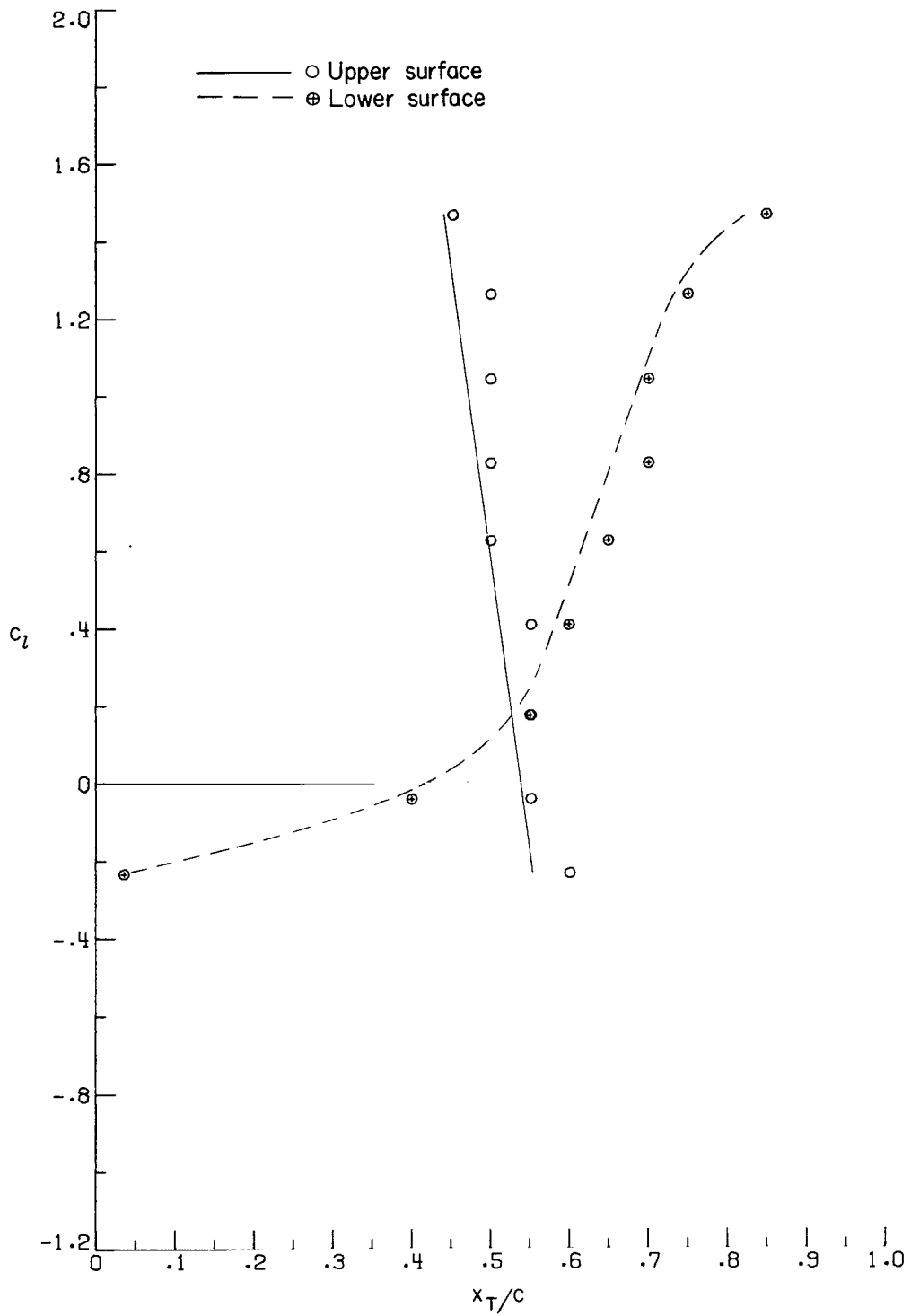
(a) $R \approx 0.5 \times 10^6$; $M = 0.05$.

Figure 8.- Variation of section lift coefficient with transition location.
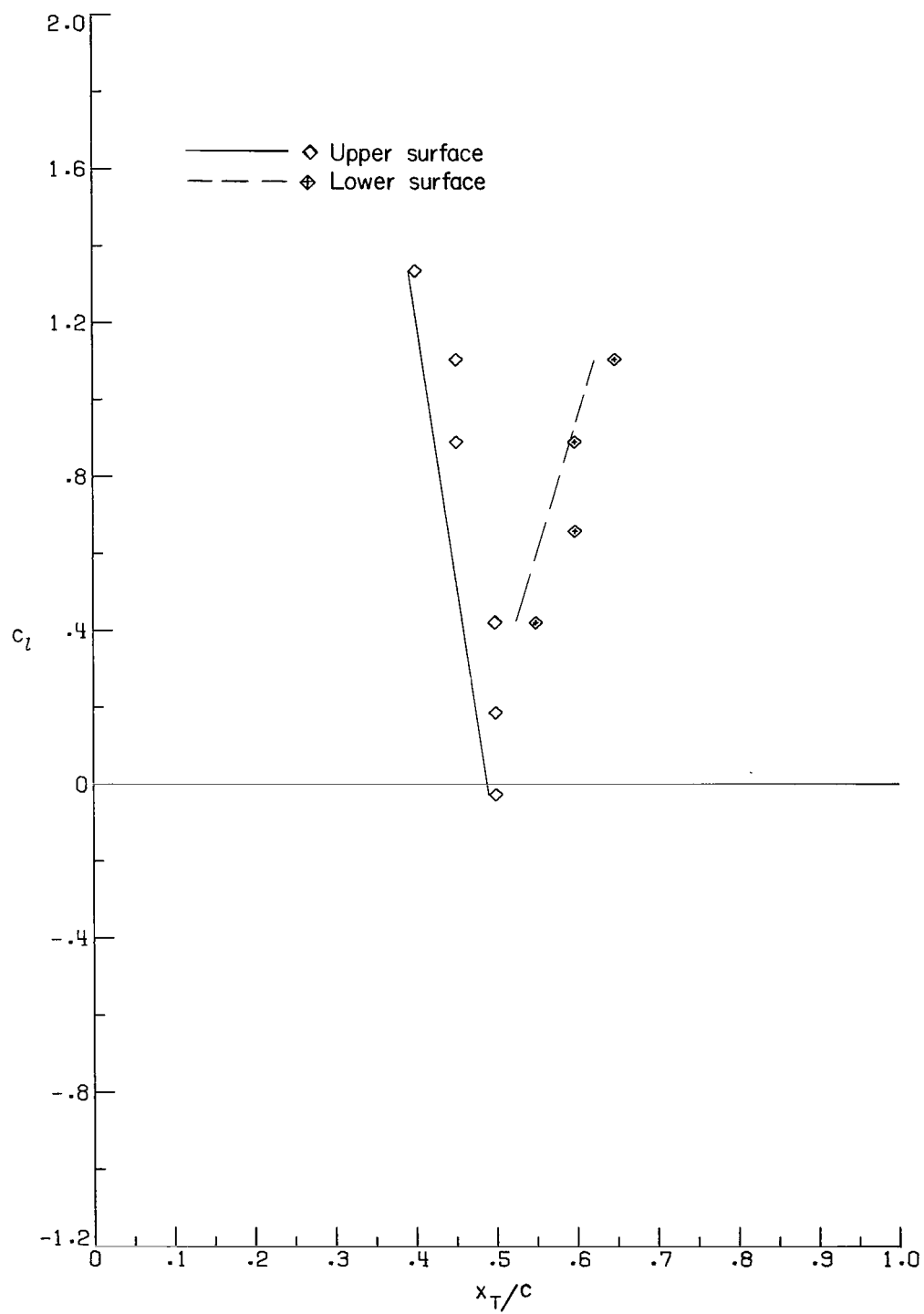
(b) $R \approx 1.5 \times 10^6$; $M = 0.15$.

Figure 8.- Concluded.
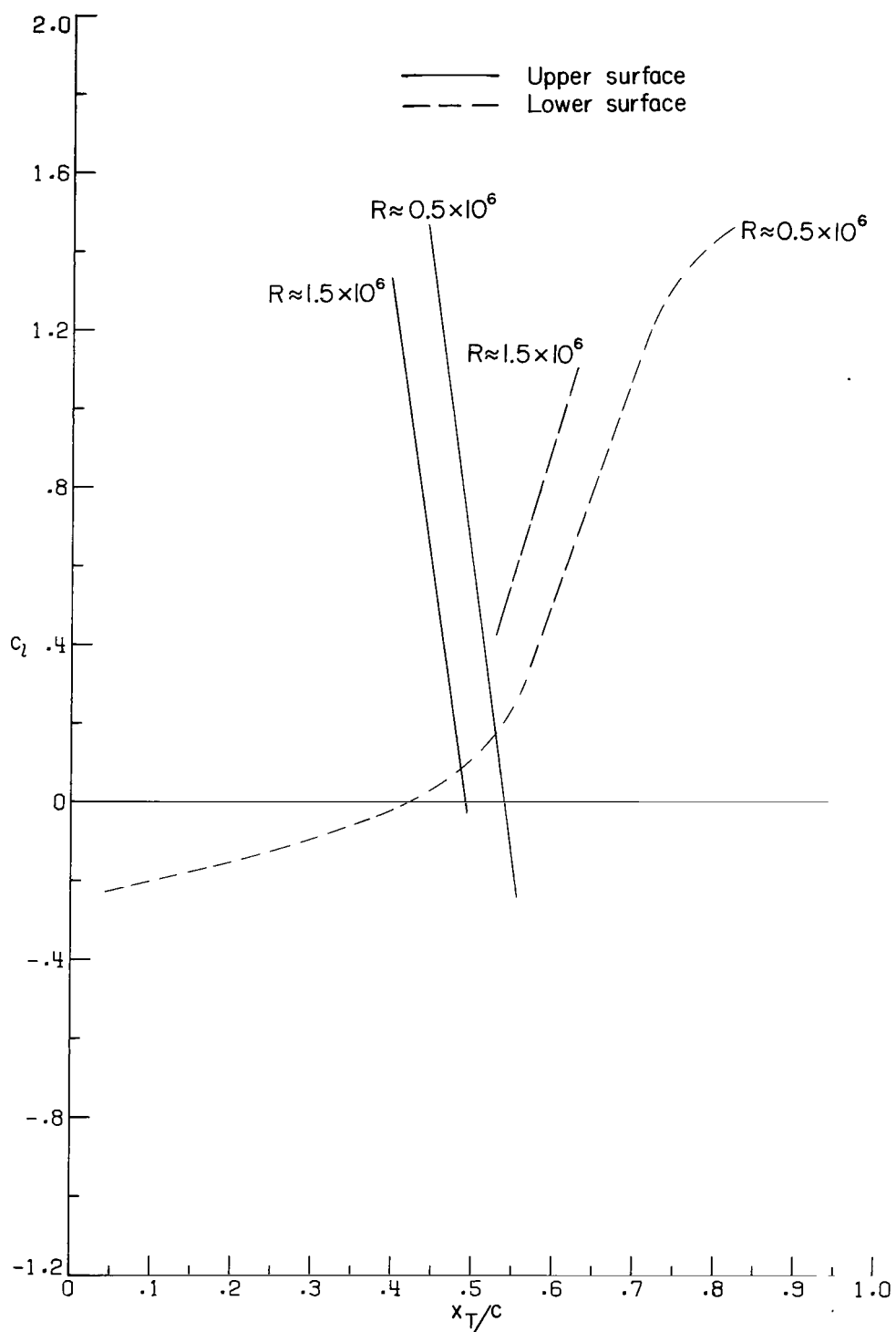
Figure 9.- Effect of Reynolds number on transition location.
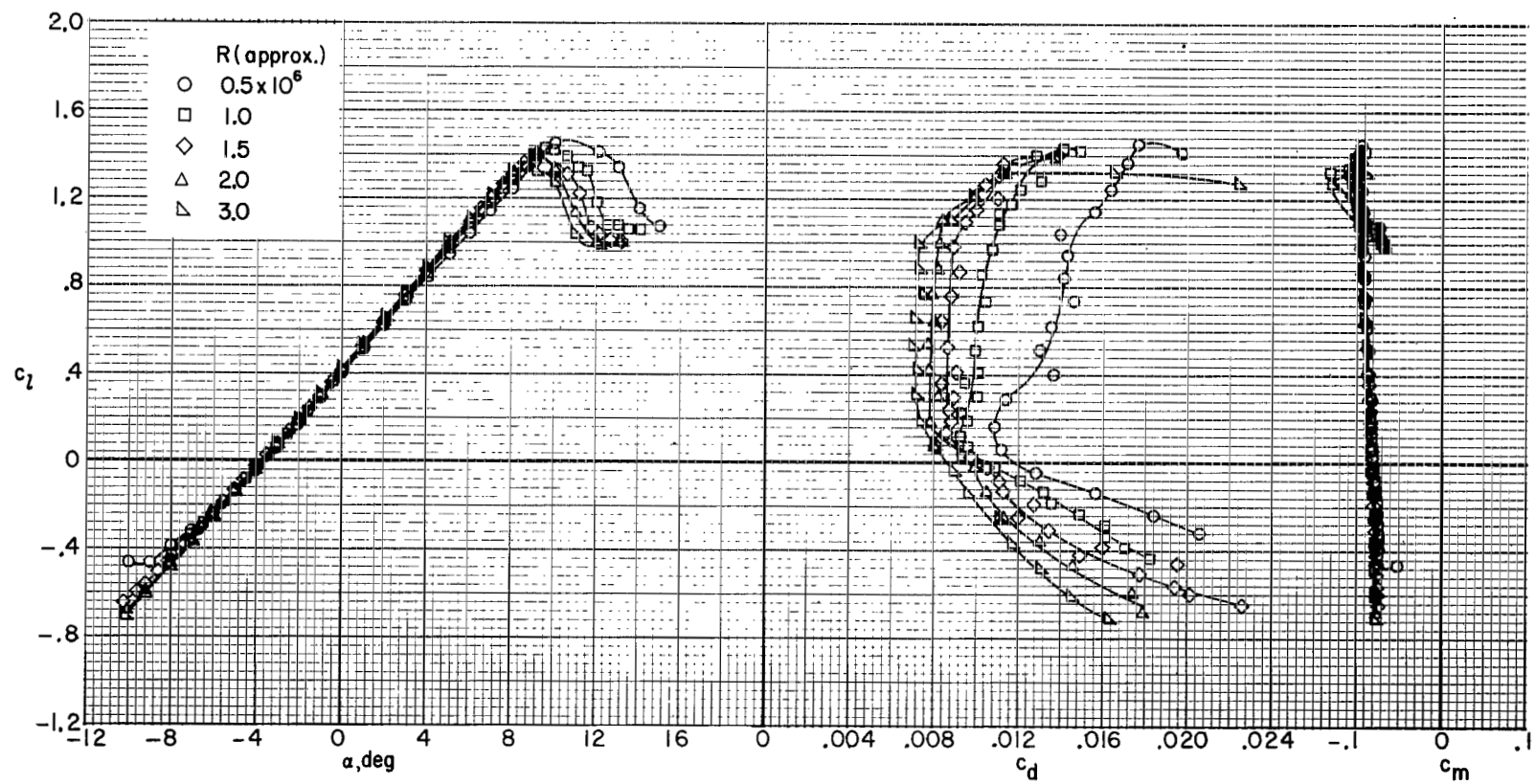
Figure 10.- Effect of Reynolds number on section characteristics at M = 0.10.
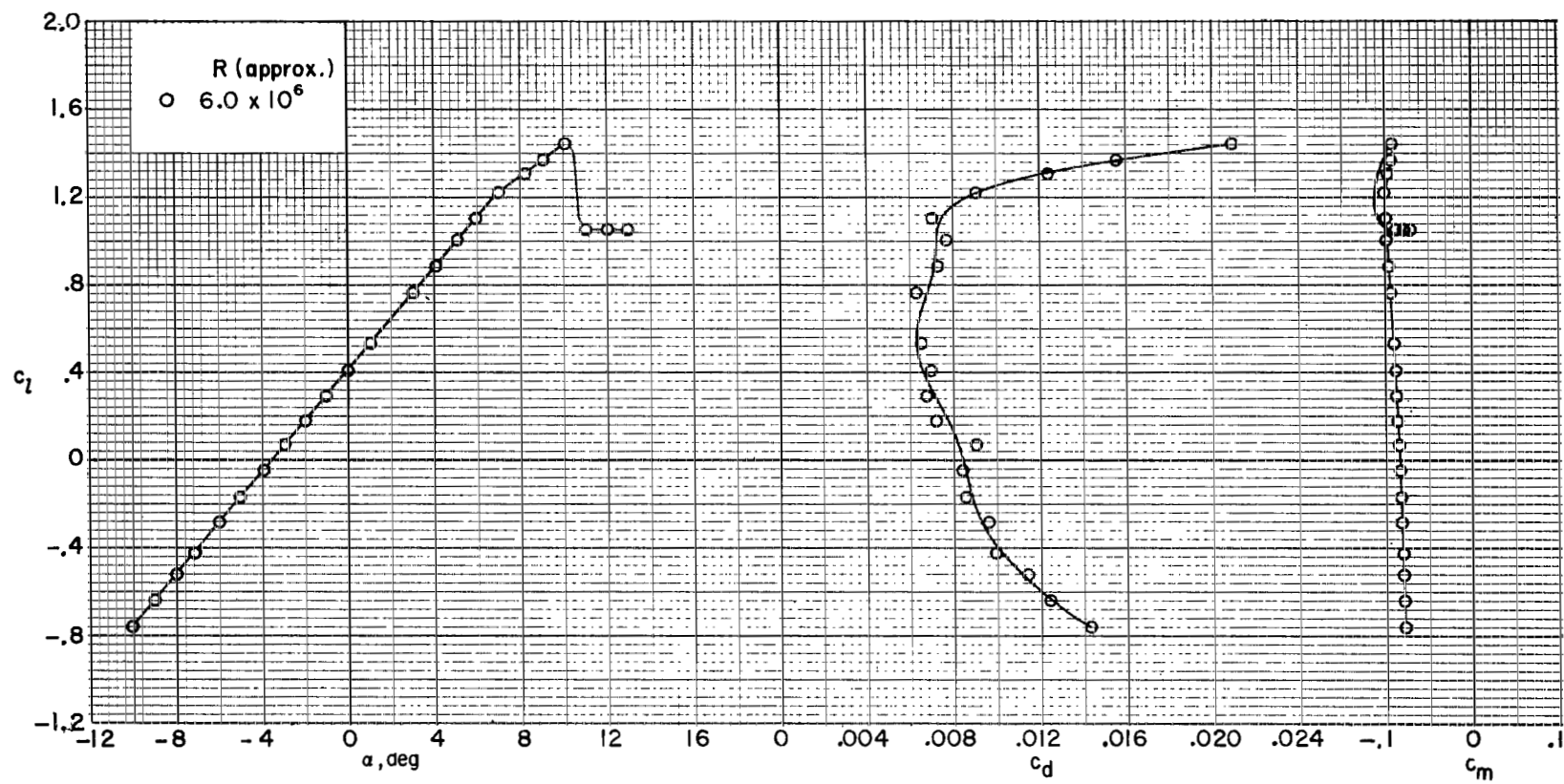
Figure 10.- Concluded.
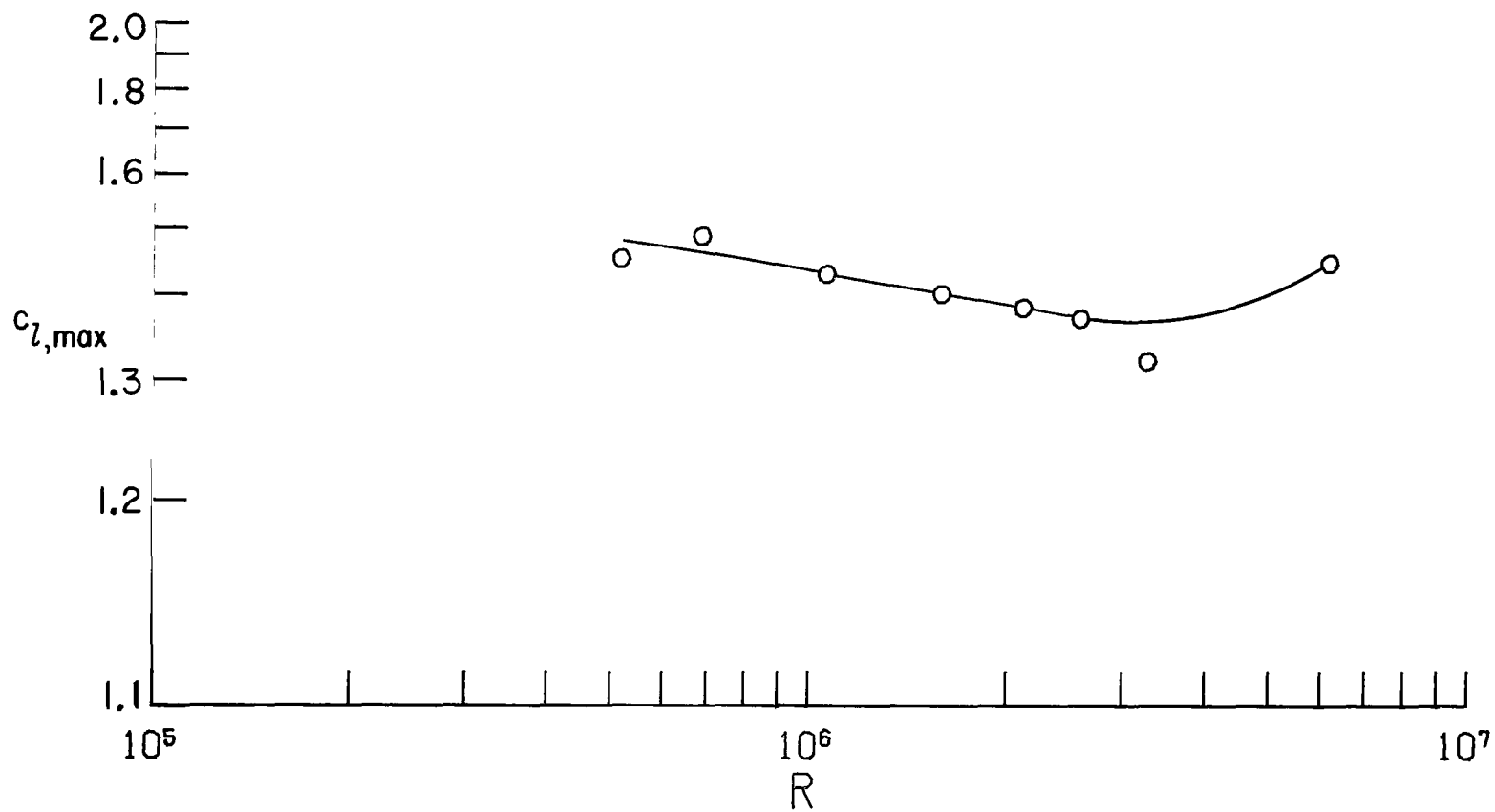
Figure 11.- Variation of maximum section lift coefficient with Reynolds number at M = 0.10.
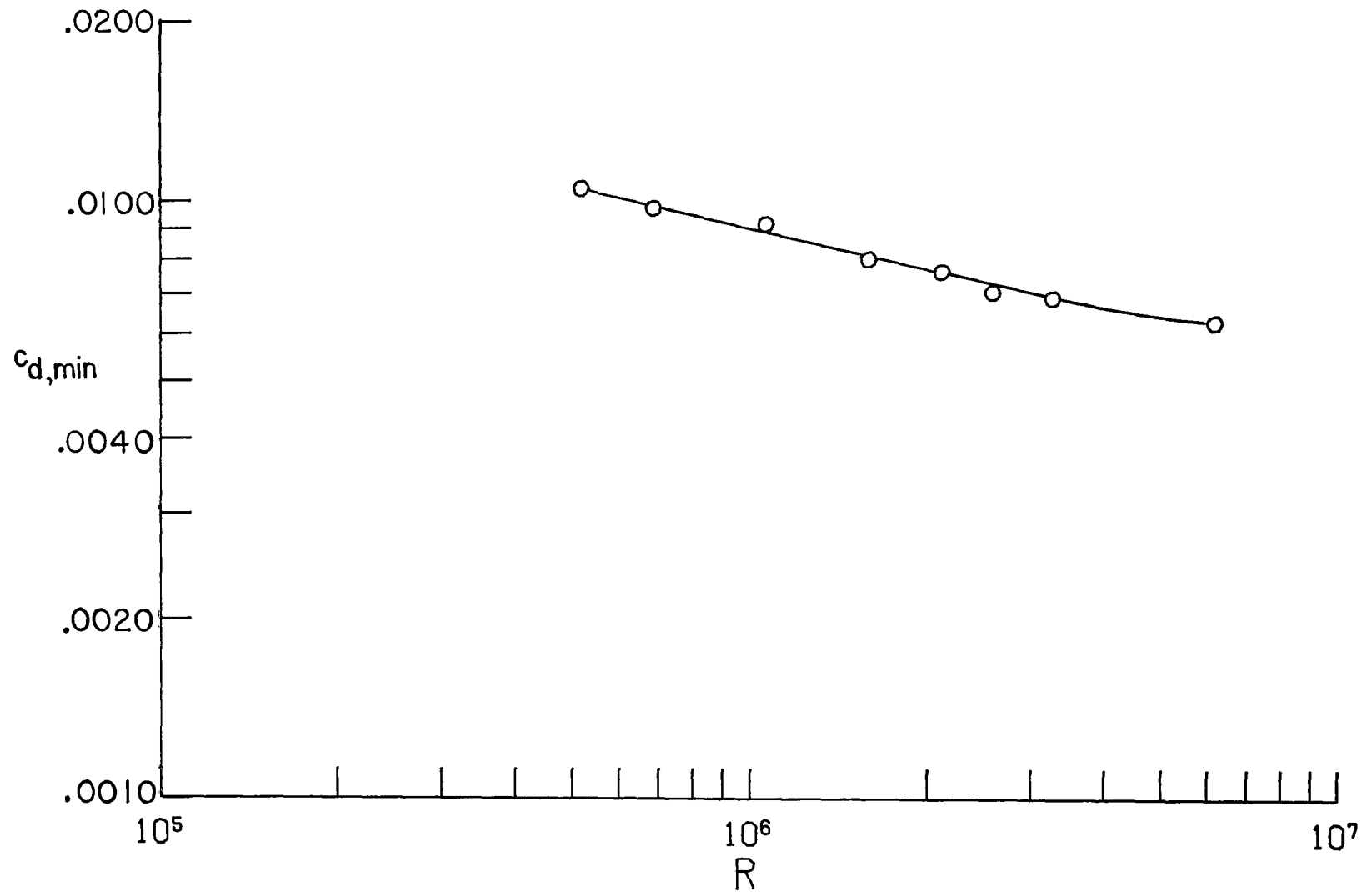
Figure 12.- Variation of minimum section drag coefficient with Reynolds number at M = 0.10.
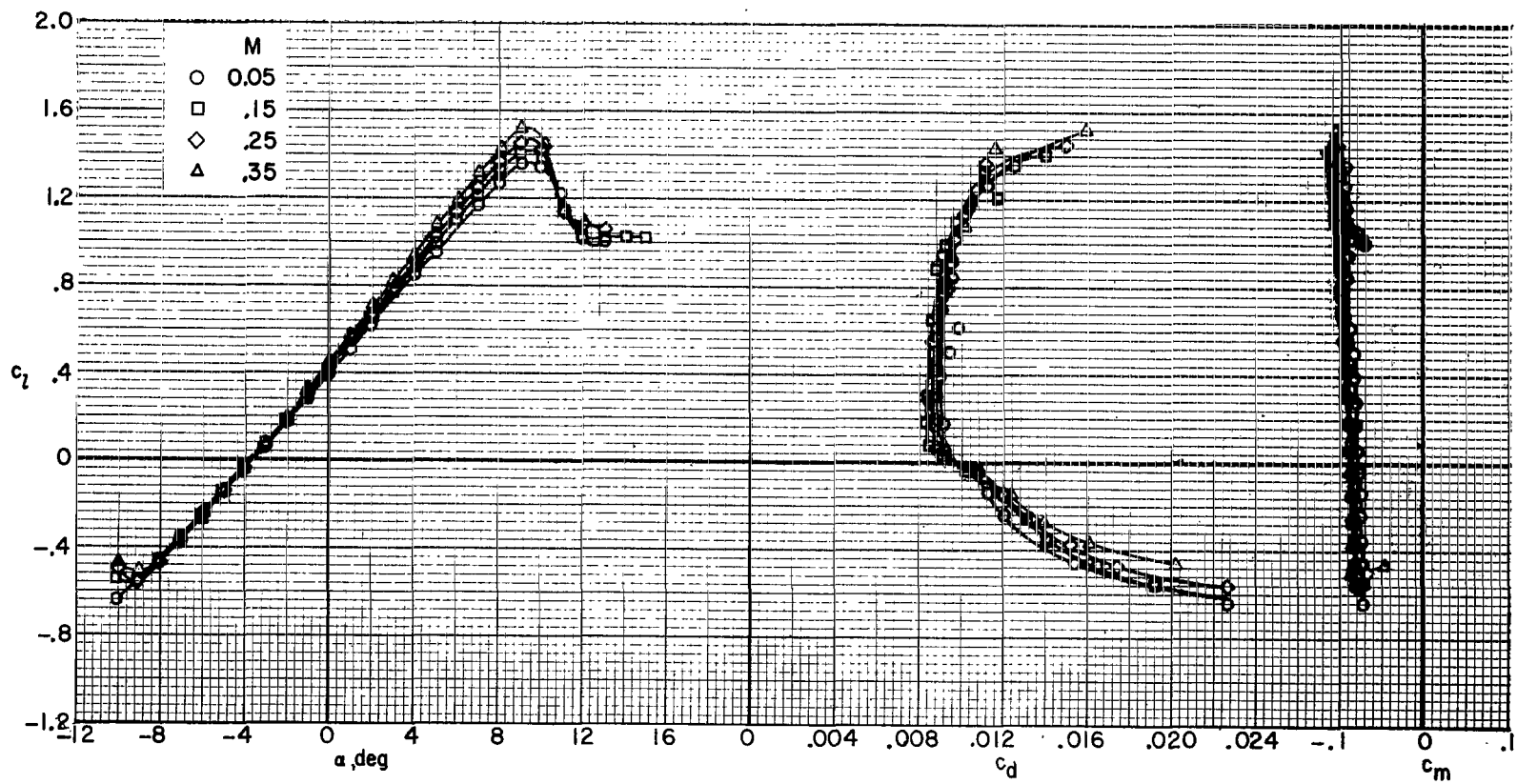
Figure 13.- Effect of Mach number on section characteristics for $R \approx 1.5 \times 10^6$.
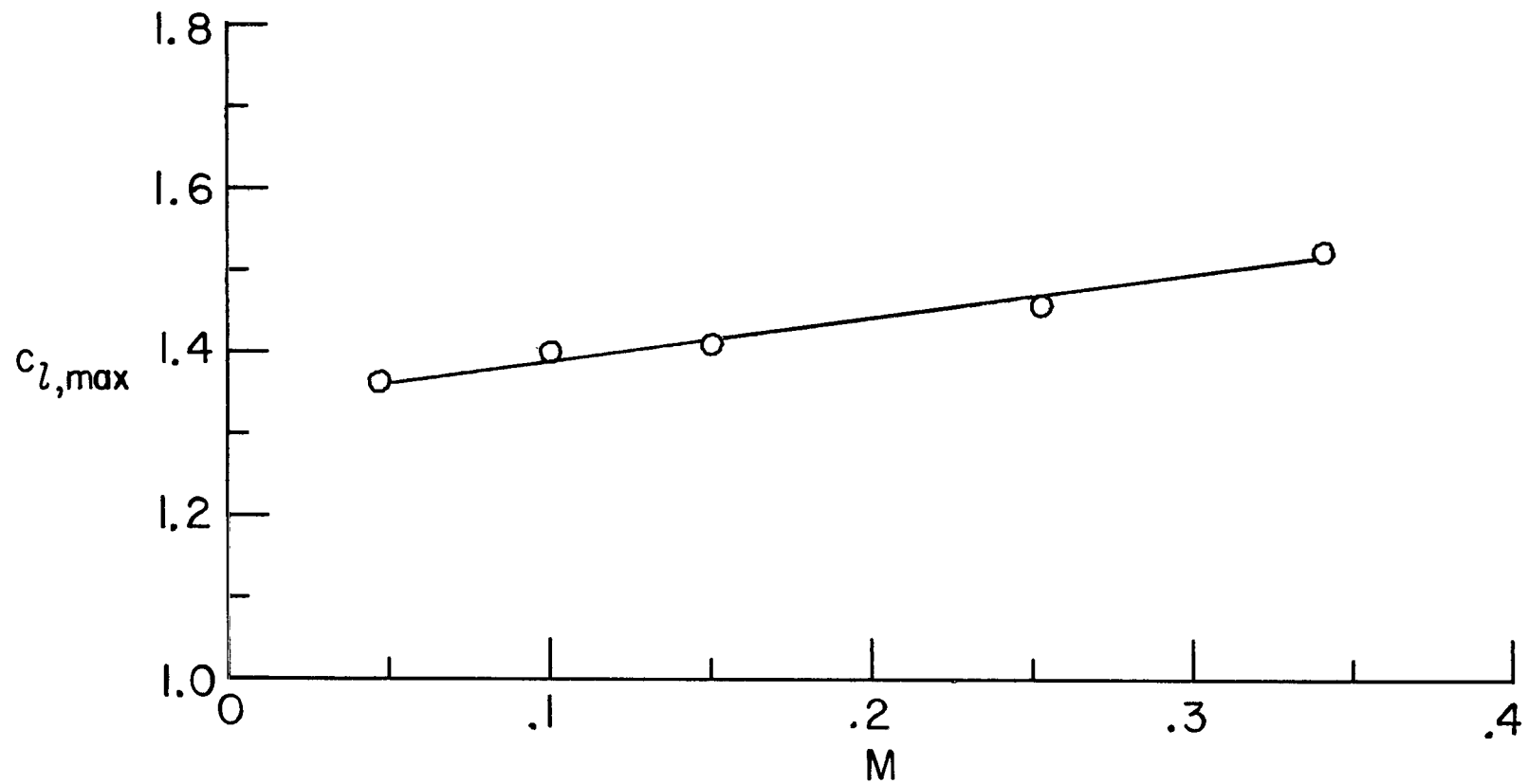
Figure 14.- Variation of maximum section lift coefficient with Mach number for $R \approx 1.5 \times 10^6$.
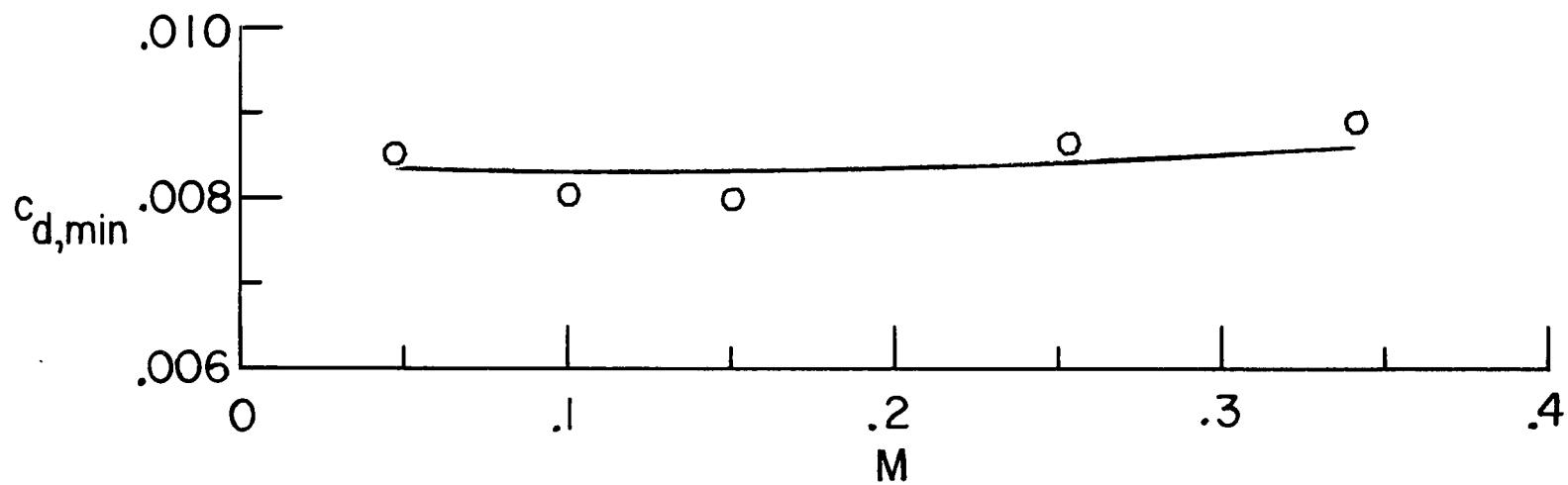
Figure 15.- Variation of minimum section drag coefficient with Mach number for $R \approx 1.5 \times 10^6$.
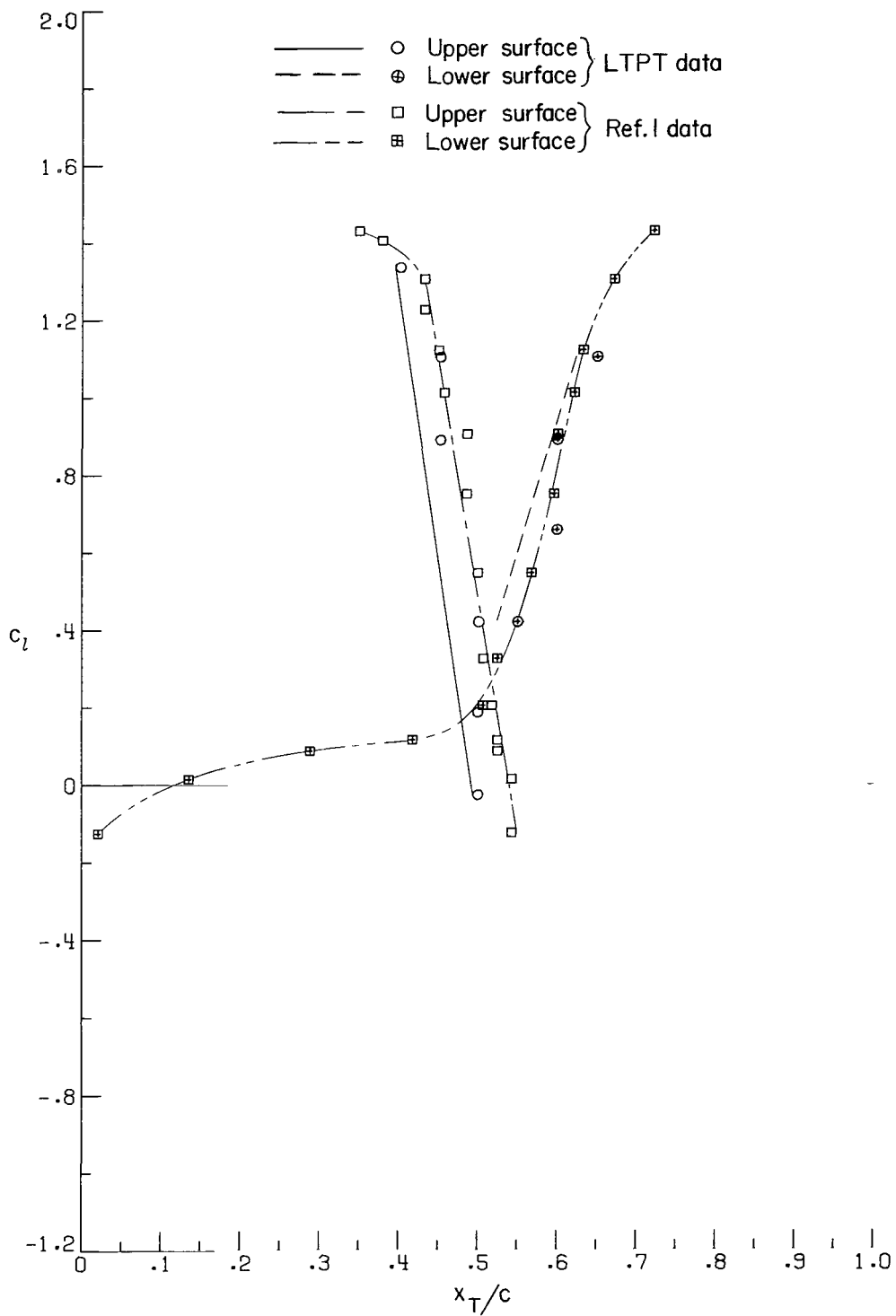
Figure 16.- Comparison of transition location on FX 66-17AII-182 (model) and FX 66-17AII-182 (design) for $R \approx 1.5 \times 10^6$.
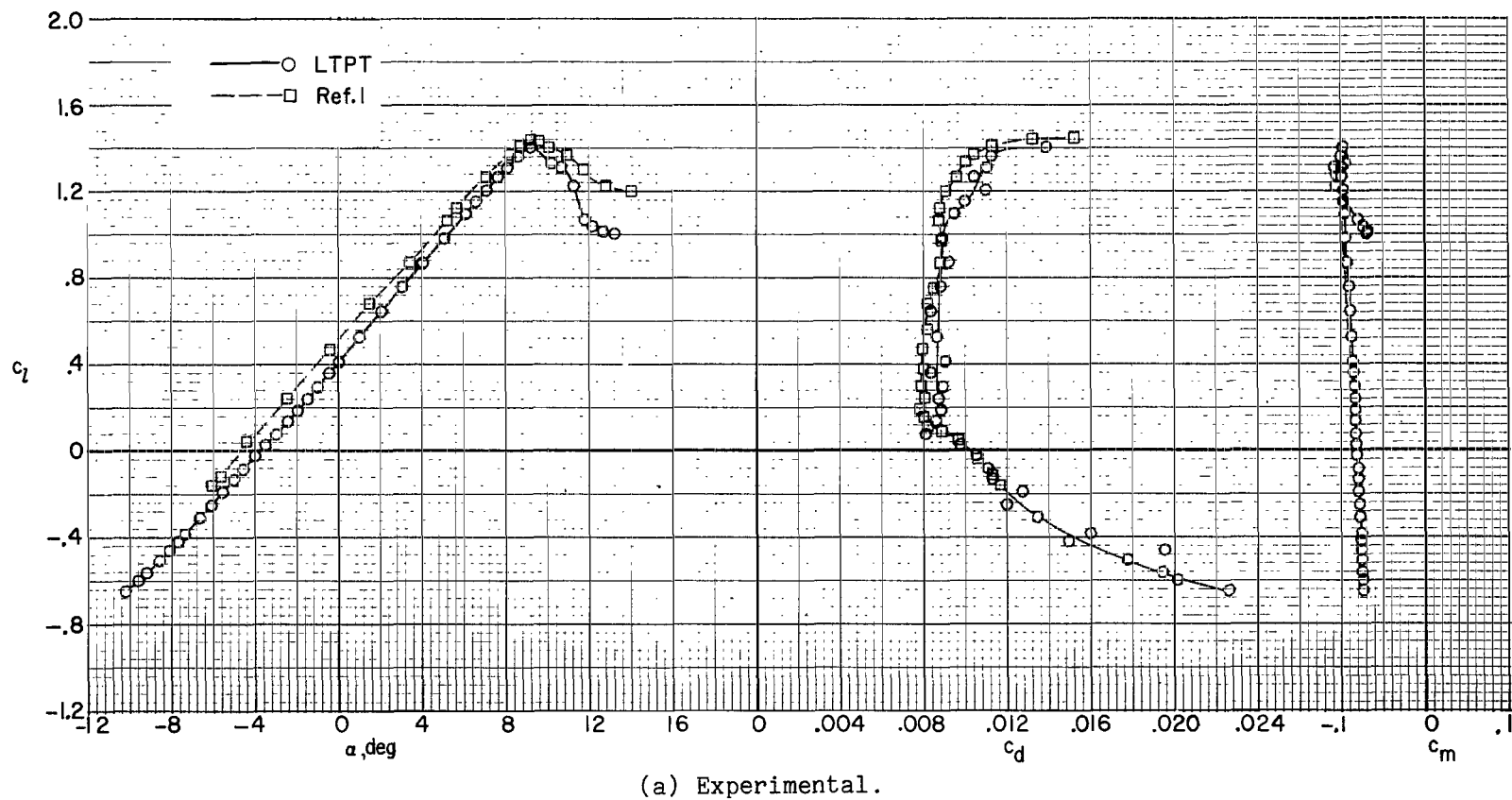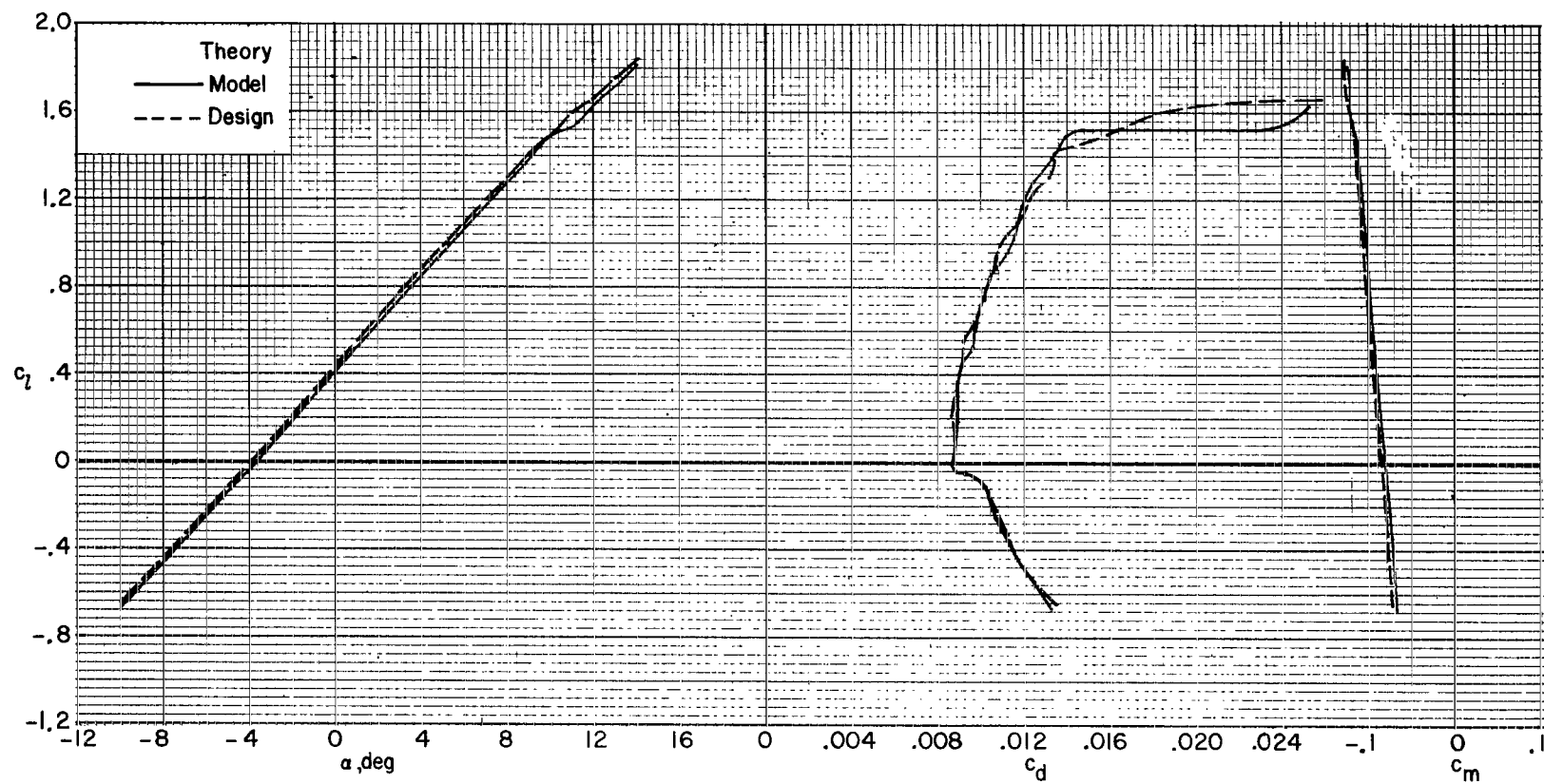
2.0

1.6

○ LTPT
□ Ref.I

1.2

.8

c_l .4

0

-.4

-.8

-1.2

-12 -8 -4 0 4 8 12 16   0 .004 .008 .012 .016 .020 .024   -.1 0 .1
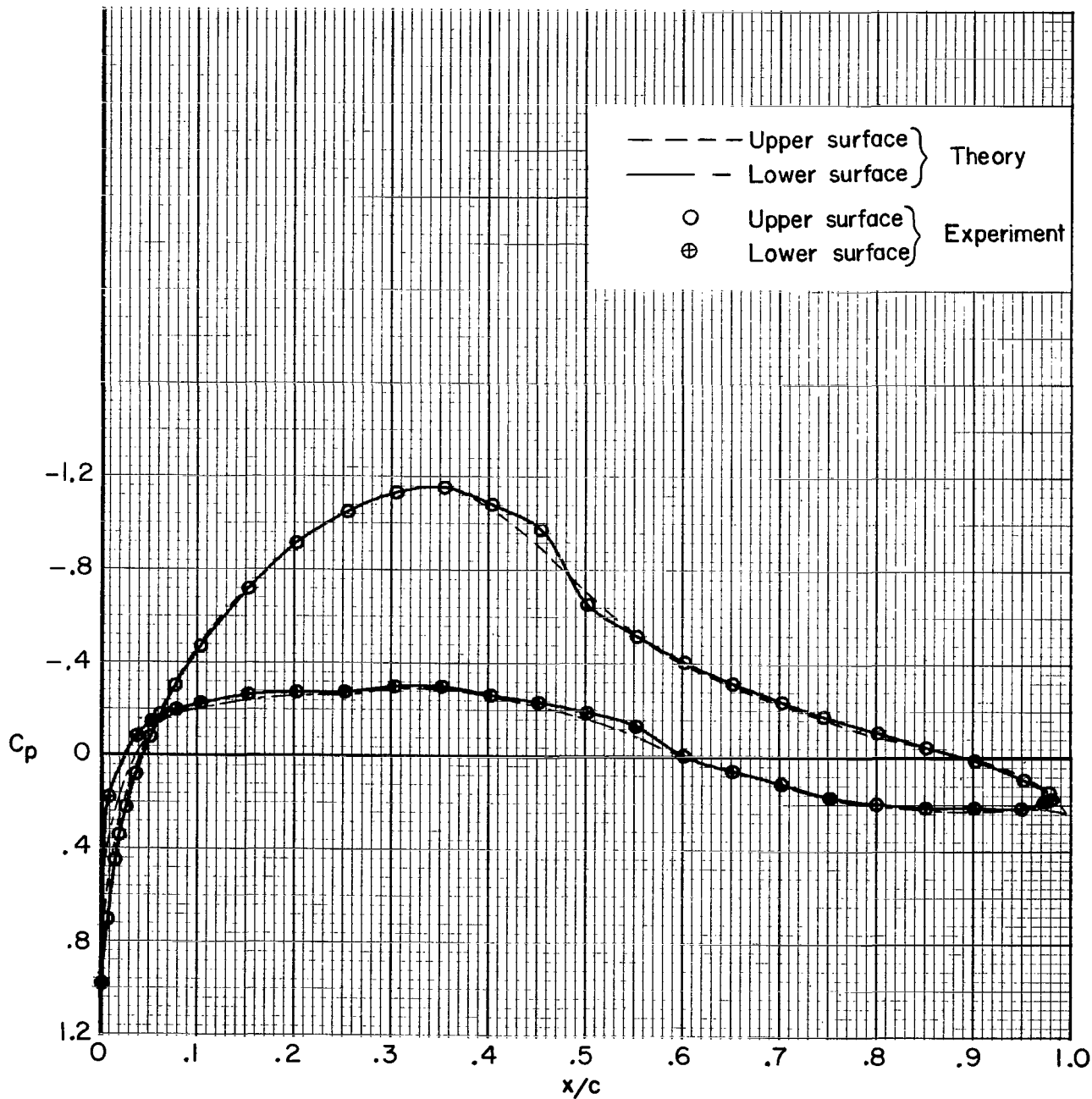
α,deg

c_d

c_m

(a) Experimental.

Figure 17.- Comparison of experimental and theoretical section characteristics
of FX 66-17AII-182 (model) and FX 66-17AII-182 (design) for $R \approx 1.5 \times 10^6$.
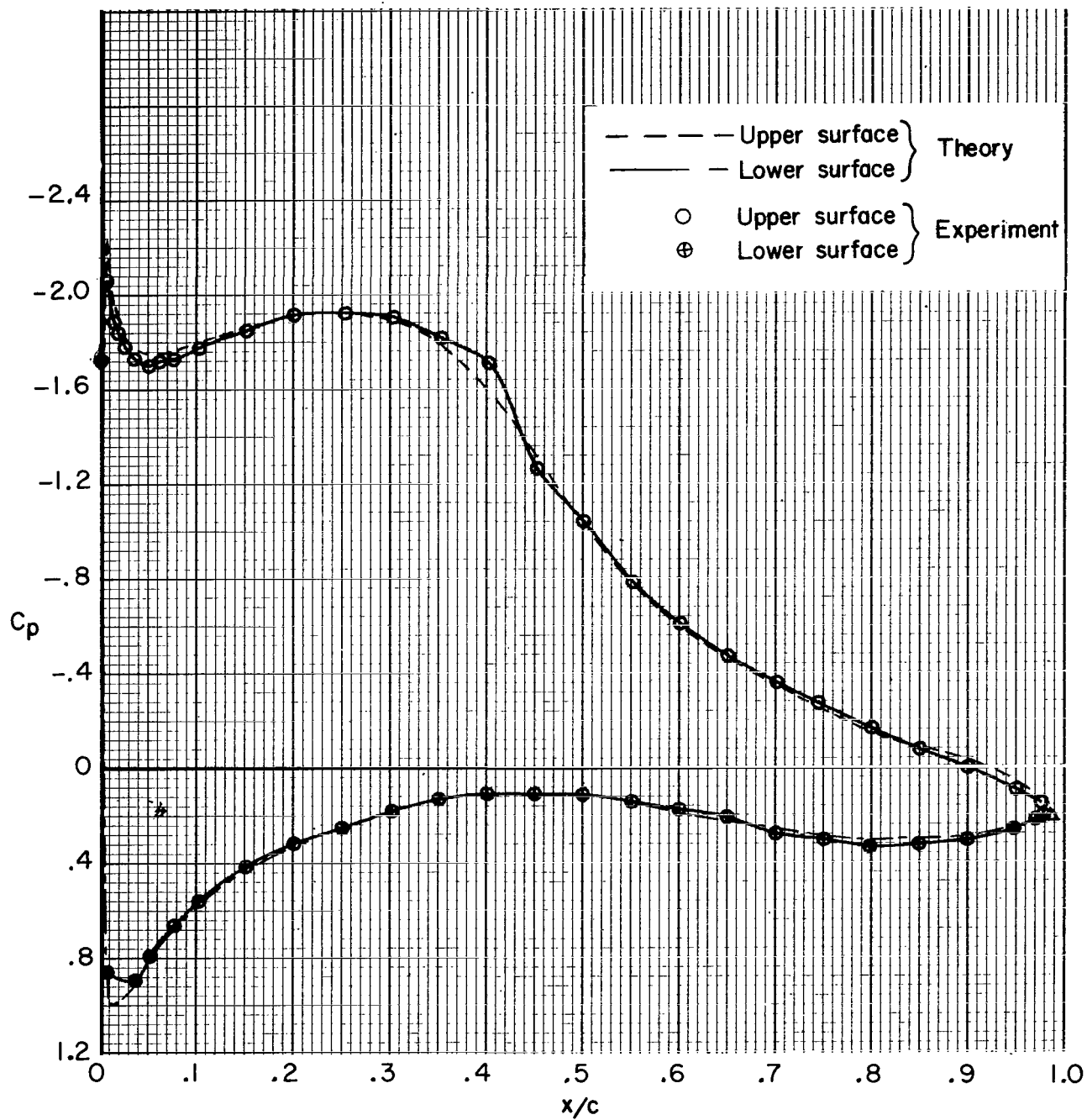
(b) Theoretical.

Figure 17.- Concluded.

(a) $\alpha = 0.00^{\circ}$.

Figure 18.- Comparison of experimental and theoretical chordwise pressure distributions for $R \approx 1.5 \times 10^{6}$ and $M = 0.10$.
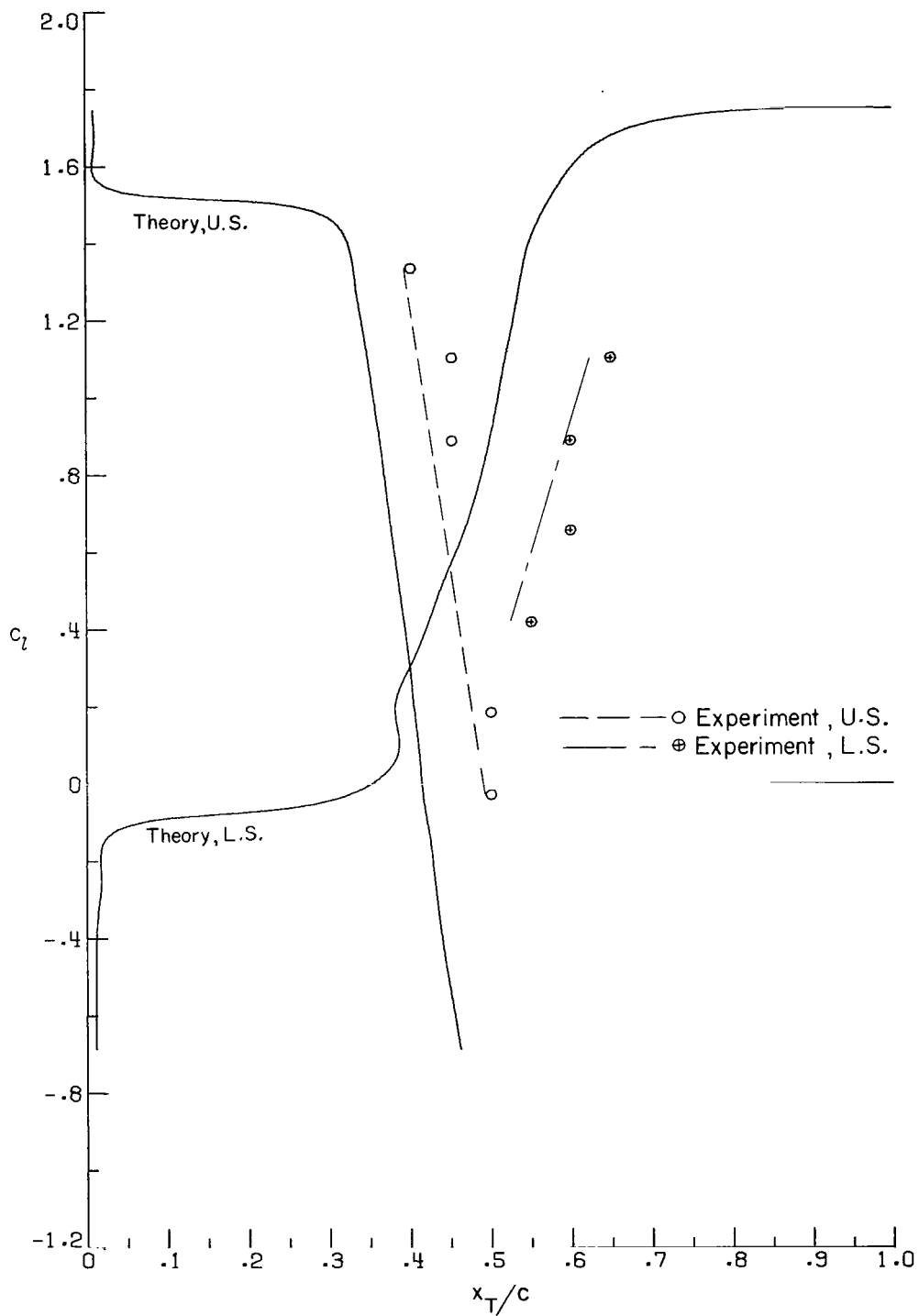
(b) $\alpha = 8.05°$.

Figure 18.- Concluded.

Figure 19.- Comparison of experimental and theoretical transition
location for $R \approx 1.5 \times 10^6$.

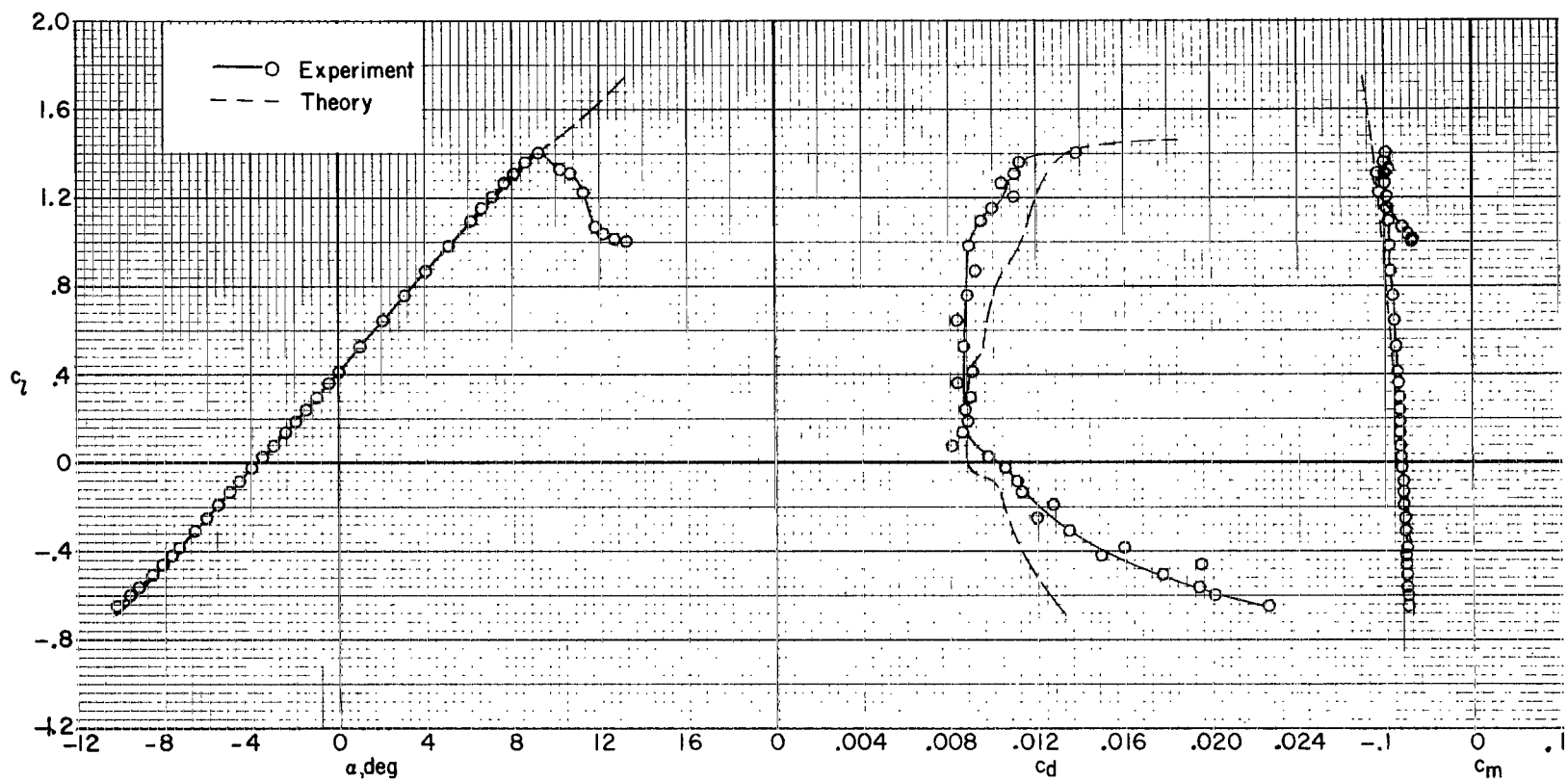Figure 20.- Comparison of experimental and theoretical section characteristics for $R \approx 1.5 \times 10^6$ and $M = 0.10$.

"The aeronautical and space activities of the United States shall be conducted so as to contribute . . . to the expansion of human knowledge of phenomena in the atmosphere and space. The Administration shall provide for the widest practicable and appropriate dissemination of information concerning its activities and the results thereof."
—NATIONAL AERONAUTICS AND SPACE ACT OF 1958

NASA SCIENTIFIC AND TECHNICAL PUBLICATIONS

TECHNICAL REPORTS: Scientific and technical information considered important, complete, and a lasting contribution to existing knowledge.

TECHNICAL NOTES: Information less broad in scope but nevertheless of importance as a contribution to existing knowledge.

TECHNICAL MEMORANDUMS: Information receiving limited distribution because of preliminary data, security classification, or other reasons. Also includes conference proceedings with either limited or unlimited distribution.

CONTRACTOR REPORTS: Scientific and technical information generated under a NASA contract or grant and considered an important contribution to existing knowledge.

TECHNICAL TRANSLATIONS: Information published in a foreign language considered to merit NASA distribution in English.

SPECIAL PUBLICATIONS: Information derived from or of value to NASA activities. Publications include final reports of major projects, monographs, data compilations, handbooks, sourcebooks, and special bibliographies.

TECHNOLOGY UTILIZATION PUBLICATIONS: Information on technology used by NASA that may be of particular interest in commercial and other non-aerospace applications. Publications include Tech Briefs, Technology Utilization Reports and Technology Surveys.

Details on the availability of these publications may be obtained from:

SCIENTIFIC AND TECHNICAL INFORMATION OFFICE

NATIONAL AERONAUTICS AND SPACE ADMINISTRATION

Washington, D.C. 20546